UC Berkeley
UC Berkeley Electronic Theses and Dissertations

Title

Precise spatiotemporal control of voltage-gated excitability in neural dendrites

Permalink

https://escholarship.org/uc/item/8v6903d7

Author

Fedorchak, Alexis Voorheis

Publication Date

2015

Peer reviewed|Thesis/dissertation

Precise Spatiotemporal Control of Voltage-Gated Excitability in Neural Dendrites

by

Alexis Voorheis Fedorchak

A dissertation submitted in partial satisfaction of the

requirements for the degree of

Joint Doctor of Philosophy
with University of California, San Francisco

in

Bioengineering

in the

Graduate Division

of the

University of California, Berkeley

Committee in charge:

Professor Richard H. Kramer, Chair
Professor Daniel E. Feldman
Professor Christoph E. Schreiner

Fall 2015

Abstract

Precise Spatiotemporal Control of Voltage-Gated Excitability in Neural Dendrites

by

Alexis Voorheis Fedorchak

Doctor of Philosophy in Bioengineering

University of California, Berkeley

Professor Richard H. Kramer (Chair)

Neural dendrites continually prove to harness more computational complexity than previously thought. The voltage-gated ion channels distributed throughout a dendritic tree are key determinants of dendritic excitability and computation. However, little is known about the specific functional impacts of voltage-gated excitability in discrete dendritic regions. Recently, an optical revolution in neuroscience has yielded a vast array of optical tools for functional interrogation of neurons and neural circuits. One such tool, Quarternary-ammonium Azobenzene Quarternary-ammonium (QAQ), is an optically-controllable small-molecule drug that affects voltage-gated ion channels. In its *trans* conformation, which is photo-inducible with green light, QAQ directly blocks all voltage-gated ion channels tested, but rapidly un-blocks those channels when converted to its *cis* form with near-ultraviolet light (Mourot et al. 2012). It does not photo-bleach, and can be robustly photoswitched back and fourth to either block or unblock channels in a matter of milliseconds. QAQ is a promising tool to control voltage-gated excitability in neural dendrites with the spatiotemporal precision of light.

In this thesis we use QAQ to rapidly, reversibly, and locally control voltage-gated ion channel activity in neural dendrites using targeted light. A wealth of experimental evidence using traditional pharmacology is already available about specific voltage-gated ion channels in CA1 pyramidal cells, so we first apply QAQ via a patch-pipette to CA1 pyramidal cells and confirm that it works as expected in a whole-cell. We find that *trans*-QAQ blocks somatic action potentials, blocks dendritic calcium activity, and enhances EPSP summation. These are all processes driven by QAQ-sensitive voltage-gated ion channel types that either boost (sodium and calcium channels) or dampen (potassium channels) intrinsic excitability.

We then investigate the level of spatial control we can achieve with QAQ using dendritic calcium imaging. Indeed, for up to three seconds after photo-switching the molecule, control is extremely precise. With this knowledge, we use local block of voltage-gated ion channels and calcium imaging to confirm and extend previous findings that voltage-gated calcium channel activity is relatively uniform throughout the apical dendritic tree of CA1 pyramidal cells. Finally, we specifically photo-control voltage-gated ion channels in the apical dendrites of CA1 neurons to experimentally probe whether dendrite-specific voltage-gated excitability affects the degree of action potential back-propagation. We find that dendritic voltage-gated ion channels determine whether a CA1 pyramidal neuron will undergo strong or weak back-

propagation, a notion that has only previously been modeled.

Contents

List of Figures

List of Tables

Acknowledgements

1. Introduction

1.1. Dendritic excitability

In the central nervous system, neurons are the cells that communicate with one another through chemical and electrical means to give rise to perceptions, thoughts, and actions. In the late 1800s, Ramon y Cajal first stained a neuron to observe its structure. What he found was that neurons are quite varied in appearance. Each neuron usually contains a soma, dendrites, and an axon, but each of these structures has incredibly different morphologies. Cajal hypothesized that information in a nervous system enters the dendrites, flows to the soma, and out the axon. In the years since, his hypothesis proved to be true. For a while, it was generally accepted that the advantage of having dendrites was simply to allow a cell to fan out spatially and form many synapses with axons passing through the area. Dendrites were thought to passively relay synaptic information to the soma, which then produced an all-or-none regenerative action potential.

Decades later, various scientists called this view into question. Field potential recordings offered the first evidence for regenerative events in dendrites (Andersen 1960; Fujita & Sakata 1962; Llinás et al. 1968; Spencer & Kandel 1961; Purpura & Shofer 1965). Then, direct recordings from the inside of dendrites then confirmed the existence of regenerative currents in alligator purkinje neurons (Llinas & Nicholson 1971), and in bits of CA1 pyramidal cell dendrite on a coverslip (Wong et al. 1979). At the same time, Wilifrid Rall extended an existing computational modeling framework for axons to dendrites (Rall 1959), then updated this framework by incorporating discrete compartments to enable theoretical studies of non-linear dendritic events (Rall 1964). Rall's compartmental model has since been influential in studies of dendritic function, by enabling researchers to make predictions and test experimental observations. In 1994, when whole-cell patch-clamping had been extended to dendrites (Stuart et al. 1993), Greg Stuart and Bert Sakmann simultaneously patch-clamped the dendrite and soma of a single layer 5 cortical neuron to record the first direct evidence of a somatic action potential actively propagating into the dendrites (Stuart & Sakmann 1994). This back-propagating spike was extinguished by application of the voltage-gated sodium channel blockers, QX-314 and tetrodotoxin (TTX), indicating voltage-gated sodium channels not only control spiking in the axon, but also govern action potential propagation into the dendrites (Figure 1.1). Indeed, dendrites not only contain voltage-gated sodium channels, but many other voltage-gated ion channels too.

In fact, voltage-gated ion channels (VGICs) are main determinants of dendritic excitability, meaning how readily dendrites will undergo regenerative events such as active back-propagation (London & Häusser 2005; Sjöström et al. 2010). Since those early experiments, VGICs have been been found to play roles in many dendritic computational events. In addition to L5 pyramidal cells, somatic action potentials actively back-propagate into the dendrites of CA1 pyramidal cells (Spruston et al. 1995; Waters et al. 2005), to an extent that varies even within a single cell-type (Golding et al. 2001; Bernard & Johnston 2003).
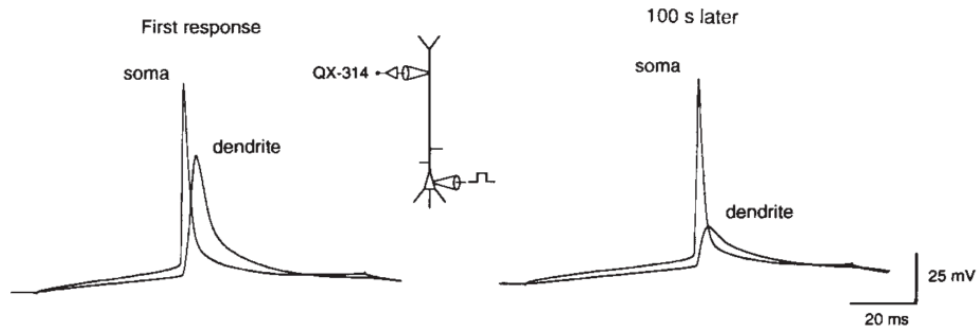
Figure 1.1: Dual recordings of a back-propagating action potential. In the first direct evidence of action potential back-propagation, whole-cell voltage recording of an action potential recorded at the soma is overlayed on the same action potential recorded 443 μm from the soma of a layer 5 pyramidal cell. After the sodium channel blocker, QX-314 diffuses into the dendrite (100 s later), the dendritic potential is greatly diminished, implicating voltage-gated conductances in dendritic back-propagation. Figure adapted from Stuart et al 1994.

An even more recent view of dendrites is that single dendritic branches may function as independently excitable units within a neuron, much like single neurons function in a circuit (Branco & Häusser 2010; Figure 1.2). Such multiple layers of single-neuron complexity creates a much richer computational landscape than previously thought (Häusser & Mel 2003). Studies have shown that in some cases activity occurring in individual branches never even reaches the soma or produces an action potential (Miyakawa et al. 1992; Wei 2001; Ariav et al. 2003; Polsky et al. 2004; Gasparini & Magee 2006; Losonczy & Magee 2006). These isolated dendritic computations are also observed in vivo (Kamondi et al. 1998; Remy et al. 2009; Smith et al. 2013) and during behavior (Xu et al. 2012; Smith et al. 2013; Palmer et al. 2014), suggesting that they hold a practical relevance.

Using traditional pharmacology, manipulations of voltage-gated ion channel activity in an entire cell have revealed a vast web of dendritic computations controlled by specific types of voltage-gated ion channels (Remy et al. 2010; Brunel et al. 2014). While sodium channels boost back-propagating action potentials along pyramidal cell dendrites, potassium channels dampen and sharpen these back-propagating signals (Stuart & Sakmann 1994). Both sodium and calcium channels have been shown to boost coincident excitatory post-synaptic potentials (EPSPs) and underlie dendritic spikes (Markram et al. 1997; Stuart & Häusser 2001; Svoboda et al. 1997), whereas potassium channels have been shown to sharpen EPSPs (Takagi 2000), precisely control action potential timing (Fricker & Miles 2000; Ariav et al. 2003), and underlie sub-linear temporal summation of EPSPs (Cash & Yuste 1998; Margulis & Tang 1998; Cash & Yuste 1999). Voltage-gated calcium channels also provide an important source of calcium for plasticity processes in dendrites (Frick & Johnston 2005; Sjöström et al. 2010; Goldberg & Yuste 2005).
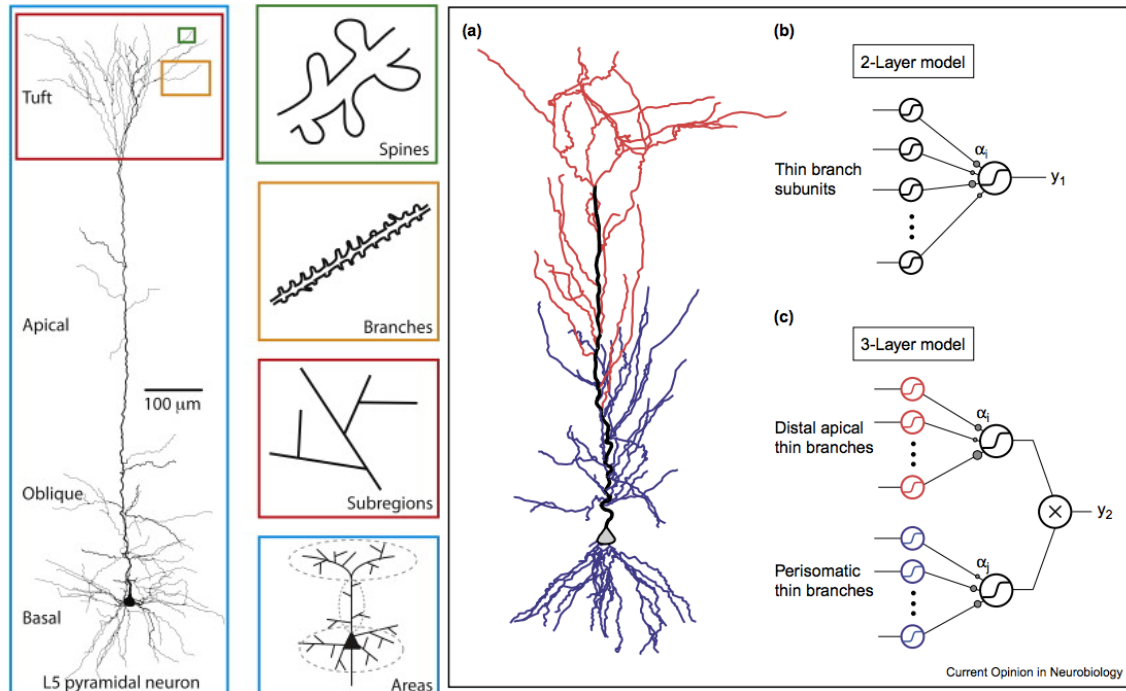
Figure 1.2. Overview of compartmentalized dendritic integration. Colored boxes on the left depict various computational layers in a pyramidal neuron (layer 5 example morphology at far left). Signals have been shown to be integrated in spines, branches, and subregions like the apical tuft, oblique dendrites, and soma. Within the large right side box: a) example morphology of a CA1 pyramidal neuron. b) Modeled idea that dendrites act as computational subunits within a 2-layered model of integration. c) Proposed scheme for multi-layered single-neuron computation. Figure adapted from Palmer 2014 & Hausser and Mel 2003.

Little is known about how the relative distribution of voltage-gated ion channels affects dendritic function. Anatomical immunolabelling and electron-microscopy have helped parse general locations of various voltage-gated ion channels in dendrites, which are found throughout all neural dendrites with considerable variation in relative levels, and channel subtypes from cell-to-cell (Migliore & Shepherd 2002; Trimmer & Rhodes 2004; Lai & Jan 2006). However, methods for localized perturbation are limited and technically challenging, so only a handful of studies have been done to address the functional profiles and computational relevance of the sub-cellular voltage-gated ion channel distributions (Figure 1.3).

a

Mitral cells

Dendritic distribution relative to somatic density (arbitrary units)

K$_A$	CaT
Na$^+$	CaL
I$_h$	CaN

Distance from soma (arbitrary units)

b

Neocortical layer V

Distance from soma (arbitrary units)

c

CA1

Distance from soma (arbitrary units)
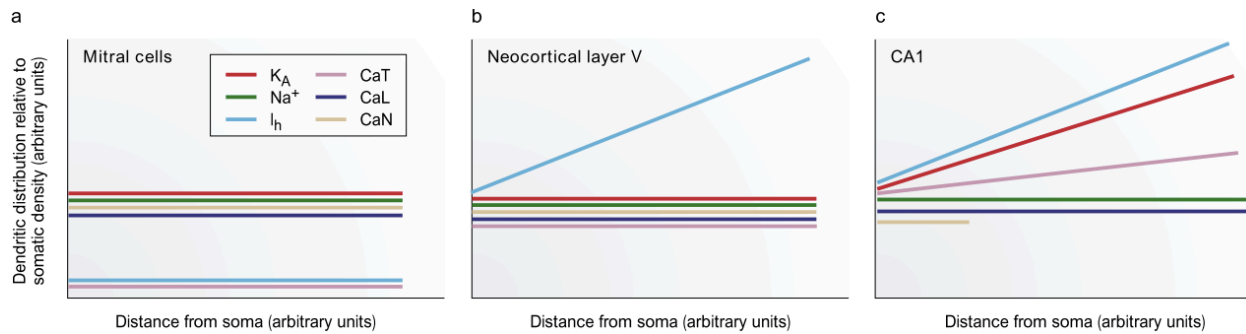
Figure 1.3: Dendritic distribution of voltage-gated ion channels. Currently we have only a low-resolution understanding of the relative distributions of the many different types of voltage-gated ion channels in neural dendrites. These simple graphs combine information gleaned from both experimental and computational studies to outline the current knowledge in the field. a) Mitral cells show relatively uniform conductances of all voltage-gated ion channels across the dendritic arbor. b) Cortical layer 5 pyramidal cells exhibit a strong gradient of increasing Ih current with distance from the soma, but relatively uniform distributions of all other channels. c) CA1 pyramidal neurons have relatively uniform distributions of calcium and sodium channels, but greatly increasing A-type potassium and Ih currents with distance from the soma. Figure adapted from Migliore & Shepherd 2002.

Dendritic patch-clamping, though low-throughput and prohibitively difficult in thin dendrites, has revealed that voltage-gated sodium and calcium channel activity is relatively uniform along CA1 hippocampal pyramidal cell apical dendrites (Magee & Johnston 1995; Bittner et al. 2012), but that voltage-gated potassium channel current increases about 16-fold from the soma to the distal dendrites (Hoffman et al. 1997; Bittner et al. 2012). Local perfusion of channel blockers is slow to act and has blurred spatial boundaries due to diffusion. But it has shown that sodium channels in the main apical dendrite boost action potential back-propagation and dendritic coincidence detection of simultaneous action potentials and EPSPs (Magee & Johnston 1997; Stuart & Häusser 2001), while potassium channels keep this coincidence activity in-check, and dampen back-propagation in oblique dendrites (Stuart & Häusser 2001; Frick et al. 2003). Further research on dendritic function will benefit from an ability to precisely control voltage-gated excitability in sub-cellular regions and individual branches.

1.2. Optical methods to manipulate neural activity.

Much has been discovered about the nervous system by simple observation. Morphological imaging studies have revealed extensive dendritic branching patterns (Chen et al. 2006; Jiang et al. 2015; Markram et al. 2015), as well as the general locations of sub-cellular structures and proteins (Trimmer & Rhodes 2004). Such studies serve a purpose to constrain our view of how the nervous system gives rise to behavior and perception, but to really uncover the basis of neural processing one must establish cause-and-effect relationships between functional mechanisms and neural outputs. We can do this by carefully manipulating certain aspects of a system, rather than simply observing. As mentioned already, methods to manipulate neural activity can be sloppy and imprecise. Electrical stimulation non-specifically targets all electrically active membranes in a certain

spatial vicinity with no regard to specific types of cells. Pharmacology allows us to manipulate specific types of ion channels and proteins to isolate the effect each channel has in general, but targeting drugs to specific areas of a dendrite to determine the localized role a channel plays in neural processing is prohibitively difficult.

In the past decade or so, a number of optical tools to precisely manipulate both neural circuits and sub-cellular function have emerged. Chemically caged neurotransmitters have a chemical group that can be cleaved (uncaged) by illumination with specific wavelength light, making them available to bind to receptors on the surface of cells (Trigo et al. 2009). With these caged compounds, researchers have been able to mimic synaptic transmission and directly assay its effect on dendritic processing. For example, glutamate uncaging on dendritic spines has revealed that clusters of excitatory inputs on a single dendritic branch will produce a non-linear dendritic spike, but that inputs distributed to multiple branches summate linearly (Losonczy & Magee 2006; Yang et al. 2014). It's also revealed that dendrites preferentially respond to synaptic activity activated in specific temporal sequences (Branco et al. 2010). The ability to perform such experiments has greatly deepened our understanding of dendritic integration (London & Häusser 2005; Tran-Van-Minh et al. 2015).

In 2005, a microbial ion channel that opens with blue light to depolarize membranes was expressed in neurons and used to control their firing with light (Boyden et al. 2005). Because the power of this technique to activate genetically-targeted neurons with light was unparalleled in specificity, it kicked off an entirely new field called optogenetics. Researchers have since developed an incredible variety of tools along this same vein, from channels that will hyperpolarize membranes and silence neurons (Zhang et al. 2007; Chow et al. 2010), to tools that are faster or have different kinetics (Yizhar et al. 2011), to red-shifted varieties that can be multiplexed together (Lin et al. 2013; Klapoetke et al. 2014). These optical tools have already been used extensively to dissect neural circuits at a level never before attainable (Deisseroth 2015).

Jumping one level down from the systems to the cellular neuroscience level, another transformative method of optical perturbation is a bit a mix of both optogenetics and endogenous control of neural receptors like with optical uncaging. Optogenetic pharmacology is a class of research tools that add a cysteine point mutation to endogenous membrane proteins such that a synthetic photoswitchable ligand will covalently attach itself to the proteins. These tools allow genetically-targetable optical control of specific neural ion channel and receptor subtypes, like block of Kv3.1 potassium channels (Fortin et al. 2011), activation of ionotropic glutamate receptors (Volgraf et al. 2006; Szobota et al. 2007), block of nicotinic acytylcholine receptors (Tochitsky et al. 2012), or block of GABAa receptors (Lin et al. 2014; Lin & Tsai et al. 2015).

Lastly, another method that's been developed is very simple. In 2008, Dirk Trauner and Richard Kramer's labs collaborated to develop single-component, non-genetic optical methods to control activity, termed optopharmacology (Fortin et al. 2008; Banghart et al. 2009). Taking known pharmacological blockers, the labs attached a reversibly photoisomerizable chemical, azobenzene. The first of these chemicals, termed AAQ, has been uniquely used to restore light responses to bind retinas (Polosukhina et al. 2012), and red-shifted versions have also been developed (Mourot et al. 2011).

1.3. Overview of QAQ

A recently developed addition to the optopharmacology toolbox is a small molecule named Quarternary-ammonium Azobenzene Quarternary-ammonium (QAQ) (Mourot et al. 2012). QAQ is based on the drug QX-314, which is commonly used as an intracellular sodium-channel blocker, though it has been shown to block other VGICs as well (Perkins & Wong 1995; Talbot & Sayer 1996). In QAQ, a light-sensitive azobenzene links two QX-314 molecules to create, essentially, a QX-314 molecule that is sensitive to light. It's been shown that QAQ is reversibly photoisomerized to its *cis*-form with illumination wavelengths between 360 and 390 nm, and photoisomerized back to its low energy *trans*-form with wavelengths between 480 and 540 nm (Fortin et al. 2008; Mourot et al. 2012). Azobenzene shows no photobleaching effects (Beharry & Woolley 2011), and QAQ has so far been shown to switch back and fourth between *cis* and *trans* forms indefinitely.

In it's *trans*-form, QAQ's chemical conformation is relatively straight, which allows it to block voltage-gated ion channel activity, but in its *cis*-form the molecule has a bent structure and cannot block voltage-gated ion channels (Figure 1.4). Previously in cultured cells QAQ was found to block all types of voltage-gated channels to some degree (Figure 1.4), including high-voltage activated calcium channels (L-type & N-types), sodium channels (including TTX-resistant types), and a slew of potassium channels, but not channels from other families including Kir, HCN, AMPA, and NMDA channels (Mourot et al. 2012). QAQ acts on voltage-gated ion channels from the inside of a cell and cannot cross lipid-membranes, so it's actions can be confined to a single neuron.

QAQ's reversibility, apparent immunity to photo-bleaching, and sensitivity to voltage-gated ion channels make it a great candidate for fine spatiotemporal manipulations of dendritic excitability. Such manipulations will be critical to advance our knowledge of dendritic function.
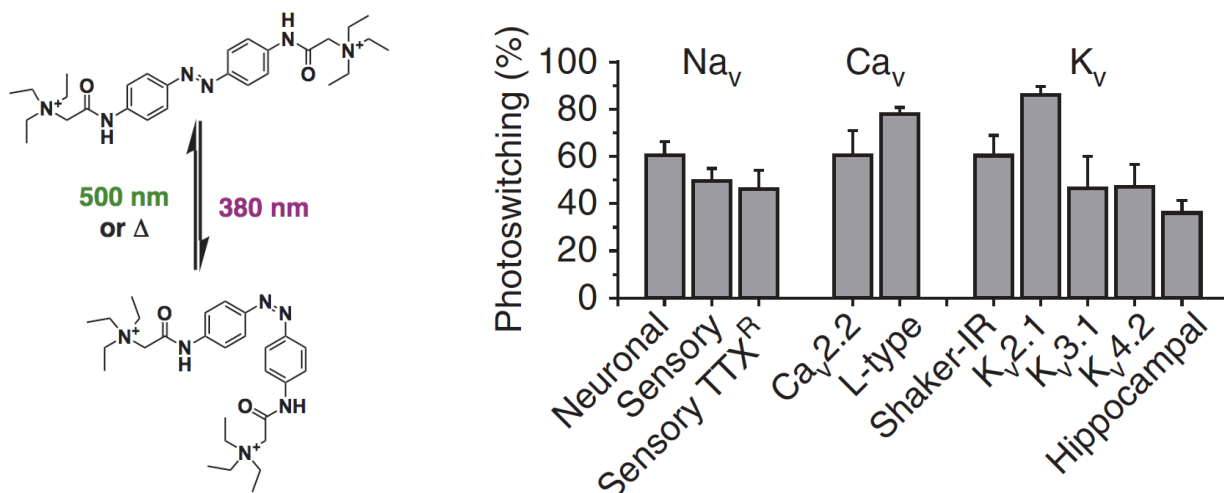
Figure 1.4: Summary of QAQ. In darkness or after absorbing green light, QAQ resides in the *trans* configuration, whereas near uv light rapidly photoisomerizes the molecule to the bent *cis* configuration. *Trans*-QAQ has been shown to block all voltage-gated ion channels tested so far (right). Photoswitching is a measure of percent current block in *trans*, calculated as $(i_{cis} - i_{trans})/i_{cis.}$ Figure adapted from Mourot et al. 2012.

1.4. Thesis preview

The goal of this thesis is to both provide a proof-of-concept that QAQ will be useful for localized functional studies of dendritic excitability, and present new biological evidence for precise roles of voltage-gated excitability in sub-cellular regions. Using QAQ, we report that ion channel block is limited to an optically-targeted area. By blocking voltage-gated excitability—essentially making a neuron passive—we confirm previous findings in CA1 pyramidal cells that voltage-gated potassium channels are dominant players in temporal summation. We also provide evidence that dendritic voltage-gated calcium channels activated during action-potential back-propagation are relatively uniform in distribution along the apical dendritic tree, and similarly distributed across both oblique and main dendrites. Finally, we offer the first experimental evidence that dendritic VGICs underlie whether CA1 pyramidal cells will display strong or weak action potential back-propagation, something that has only previously been simulated (Golding et al. 2001), and we reveal differing voltage-gated excitability profiles within each cell population.

2. Methods

We used both whole-cell patch-clamp electrophysiology, and two-photon calcium imaging to record neural activity. Here we report the materials and methods used to obtain our results.

2.1. Materials

Table 2.1: List of chemicals and reagents.

Purpose	Chemical	Source
Slicing & Recording	NaCl	Sigma-Aldrich
	KCl	
	$MgCl_2$	
	NaH_2PO_4	
	$NaHCO_3$	
	D-Glucose	
	CaCl	
	Sodium L-ascorbic acid	
	Picrotoxin	
	Gluconate	
	HEPES	
	EGTA	
	Na-GTP	
	Mg-ATP	
	KOH	
	95% O_2, 5% CO_2 tank	Praxair
	Double-distilled (DD) H_2O (>18 mOhm resistance)	Millipore
Imaging	Alexa 594	Molecular Probes
	Fluo-4	
	Fluo5f	
Optical VGIC Control	QAQ	Synthesized in-house

2.2. Solution preparation

External Solution for slicing and recording (rat tissue):
    1) Dissolve the chemicals listed in table 2.2 in ~650 mL DD H_2O.

Table 2.2: External Solution.

Chemical	Final Concentration (mM)
NaCl	126
KCl	2.5
$MgCl_2$	1.3
NaH_2PO_4	1.25
$NaHCO_3$	26
D-Glucose	10

    2) Add DD H_2O to bring solution to just under 750 mL.
    3) Check pH. If less than 7.22 pH, add ~10 μM of 8 molar KOH at a time to bring solution to 7.22-7.28 pH. If over 7.28, remake solution.
    4) Check solution osmolarity with an osmometer. If above 296 mOsmol, bring solution to between 296 and 290 mOsmol. If less than 290, remake solution.
    5) Calcium chloride should only be added after bubbling O_2 through the solution for at least 10 minutes to saturate (this ensures that all calcium will remain in solution. CaCl may form precipitate without bubbling first). For slicing, add 1 mM total CaCl. For incubation and recording, add 2.5 mM total CaCl.

        *For calcium recording experiments, we added 100 μM picrotoxin by dissolving ~6 mg/100 mL in External Solution, and mixing for ~30 minutes, or until completely dissolved.

Internal Solution for whole-cell current-clamp:
    a) Dissolve the chemicals listed in table 2.3 in ~40 mL DD H_2O.

Table 2.3. Internal Solution.

Chemical	Final Concentration (mM)
K-gluconate	116
HEPES	20
KCl	6
NaCl	2
EGTA	.5
Mg-ATP	4
Na-GTP	0.3

    b) Add DD H_2O to bring solution to ~45 mL.

c) Check pH. If less than 7.18 pH, add ~5 μM of 1 molar KOH at a time to bring solution to 7.18-7.22 pH. If over 7.22, remake solution.

d) Check solution osmolarity with an osmometer. If above 293 mOsmol, bring solution to between 287 and 293 mOsmol. If less than 287, remake solution.

e) Filter with .22 μm vacuum filter and split into 500 μL aliquots. Store at 20 °C for up to 2 months.

f) Before each day of recording, thaw one aliquot and add desired amounts of QAQ, Alexa 594, and calcium indicator dye.

2.3. QAQ preparation

QAQ was synthesized in-house as a solid powder with a TFA counter-ion. Its molecular weight is 722.2, and it is chemically stable in aqueous solution (we have used years-old aqueous stock solutions with great success). In order to ensure proper and consistent concentration from day-to-day, we made a ~20 mM aqueous stock solutions of QAQ, 500 μL at a time, then aliquoted out 5 μL portions and stored them in a -20°C freezer. Before each day of experiments, we added 5 μL of 20 mM QAQ to 1 mL internal solution for a final concentration of 100 μM QAQ in the patch pipette.

Sometimes our in-house synthesis yielded leftover silicon particulates in the QAQ-TFA powder. For this reason, after dissolving enough powder for 20 mM stock solution in DD H_2O, we always centrifuged the solution and pipetted it into a new eppendorf tube, discarding any silicon particulates that collected at the bottom of the tube after centrifuging. After removing this potential silicon debris, we checked the final concentration of our stock solution by measuring its optical density with a nanodrop (Thermo Scientific), and adjusted aliquot volumes accordingly.

2.4. Animals

Experimental procedures were performed with approval from the UC Berkeley Animal Care and Use Committee. Prior to experiments, Sprague-Dawley rats (Charles River) were housed in an Office of Laboratory Animal Care facility at UC Berkeley, kept on a 12 h–12 h light–dark cycle and had *ad libitum* access to food and water at all times.

2.5. Acute hippocampal slice preparation

Acute hippocampal brain slices were prepared as follows:

1) Prior to experiments, we cooled external slicing solution (section 2.2.1) to 4°C, and heated a water bath to 34°C.

2) Rats (P14 – P23) were deeply anesthetized using isoflurane.

3) When breathing slowed to less than 1 breath/minute we quickly decapitated the rat and dissected out the brain in chilled external slicing solution bubbled with 95% oxygen.

4) Positioned dorsal-side up on a chilled platform, we cut off the cerebellum and the frontal lobe (~rostral third of the brain) with a clean razor blade, carefully severed the midline to separate the two hemispheres, crazy-glued the brain rostral side down in a vibrotome (Leica VT1000-S), then filled the slicing chamber with chilled external slicing solution bubbled with 95% oxygen.

5) To target the hippocampus, the first slice was made starting about 2100 μM down from the surface of the tissue (caudal end up), and subsequent slices were 350 μm

thick.

6) As cut, each slice was transferred to a holding chamber filled with external recording solution (section 2.2.1), and bubbled with 95% oxygen.
7) Brain slices were incubated for ~20 min at 34 °C and stored at room temperature in an oxygenated chamber until used (up to 6 hours from slicing).

2.6. Electrophysiological procedures

For experiments using only electrical recordings, neurons were visualized with infrared Dodt-contrast imaging on an upright Olympus microscope and identified based on their morphology. For combined imaging and electrical recordings, neurons were visualized with diffuse oblique infrared light from a Dodt contrast tube (Siskiyou) positioned below the slice.

Recording pipettes (4–6 MΩ) were pulled from borosilicate glass, and filled with internal solution (section 2.2.2) containing either 100 μM QAQ and 40 μM alexa 594, or 100 μM QAQ, 40 μM alexa 549, and either 50 μM Fluo-4 or 200 μM Fluo-5f (Yasuda et al. 2004). Signals were acquired using an Axopatch amplifier (Axon Instruments), low-pass filtered at 2–3 kHz, and sampled at 30–50 kHz.

Membrane voltage was recorded under current-clamp in bridge mode. Series resistances measured between 10 and 35 MΩ, and experiments were terminated if this range was exceeded. The resting membrane potential of all cells in the results presented in this thesis was between -70 and -55 mV. This is consistent with typical resting membrane potentials of CA1 hippocampal neurons (Staff et al. 2000). If a cell's resting membrane voltage exceeded this range, or we needed to inject more than 50 pA holding current to keep membrane voltage near -60 mV, experiments were terminated. For calcium imaging experiments, resting membrane potentials remained in an even narrower range (-65 to -58 mV). This is likely because these experiments required us to hold cells for at least an hour, and cells resting outside this range typically did not last as long as necessary.

Temporal summation

To measure synaptic summation, a series of four EPSPs at 50 Hz was evoked by stimulating Schaffer collateral axons when recording in CA1 pyramidal neurons. EPSPs were recorded at the soma in presence of picrotoxin (100 μM) to block inhibitory PSPs. Temporal summation was calculated as the ratio of the amplitudes of the last and first EPSP in a train ($EPSP_4/EPSP_1$).

EPSP-spike coupling

For EPSP-spike coupling experiments, a double-barrel stimulating pipette with about a 5 μm wide tip was placed in the *stratum radiatum*. We gently moved the pipette to different positions until an EPSP was generated, then slowly increased the simulation amplitude until reliable action potential firing occurred in 390 nm light (*cis*-QAQ), then slowly decreased the stimulation amplitude back to baseline. The cell was allowed to rest for 20 seconds between each stimulation pulse, and we recorded around 100 EPSPs total during the course of one experiment to get an accurate measure of spike probability. For branch-point block EPSP-spike coupling, we first visualized the dendrites with a florescent red dye (Alexa 594), and then placed the double barrel pipette between 5 and 20 μm from an identified branch.

Step responses

For step response experiments, we injected either 120 ms (Figure 3.2), or 250 ms (Figures 3.1, 3.6, 3.7, & 3.11) with current amplitudes necessary to reach threshold varying between 25 pA and 300 pA. For plots of current vs. number of action potentials, we increased the stimulus by 50 pA above threshold with each successive step.

Back-propagating action potentials

To elicit back-propagating action potentials for calcium imaging experiments (Figures 3.8, 3.10, 3.12, 3.14, & 3.15), we injected a train of three 2-ms long current pulses into the soma at 40 Hz. The amplitude of the brief current injections was relatively high (~700-1000 pA) in order to overcome the time needed for capacitive charging to bring a neuron to threshold in just 2 ms. At the beginning of each experiment, we chose a current injection amplitude that reliably evoked spikes with each pulse. During a 40 Hz pulse train, *trans*-QAQ did not abolish subsequent action potentials in a train as it does during a step-response, but it did greatly reduce both their amplitudes and afterhyperpolarizations compared with *cis*-QAQ.

2.7. Two-photon Calcium Imaging

Set-up & calibration

Two-photon calcium imaging was performed on two separate microscope systems. Experiments in figure 3.8 were done on a home-built two-photon microscope running Scanimage software (Pologruto et al. 2003). A Chameleon Ti-Sapphire laser (Coherent, Inc.) was tuned to 810 nanometers and the laser beam was delivered through a 40x Olympus water immersion objective (.8 NA) above the slice. To control QAQ, 380 nm and 500 nm were delivered with a fiber-optic Prismatix LED through a condenser below the slice. A shutter was used to shield the photomultiplier tubes from potentially damaging light during photoswitching. Images were acquired at 25 Hz in 16 × 16-pixel frames covering 5 × 5 μm. Imaging was triggered via a TTL pulse from the electrophysiology software pClamp.

Two-photon imaging experiments in figures 3.10, 3.12, 3.14, & 3.15 were performed at 810 nm (Chameleon Ti-Sapphire laser; Coherent, Inc.) on a Moveable Objective Microscope (MOM; Sutter, Inc.) running Scanimage software (Pologruto et al. 2003). Infrared two-photon light was delivered above the slice through a 20x Olympus water immersion objective (.95 NA). Images were acquired at either 13.5 or 27 Hz in 32x32 or 16x16-pixel frames, respectively. The MOM was modified to include a Lumencore light source in the epiflorescent pathway, a TTL-controlled removable mirror to switch between wide-field epiflorescent and laser scanning light paths, and a 488 laser co-aligned with the two-photon laser (Figure 2.1). Both the home-built and MOM microscopes were equipped with electrophysiology headstages and amplifiers.
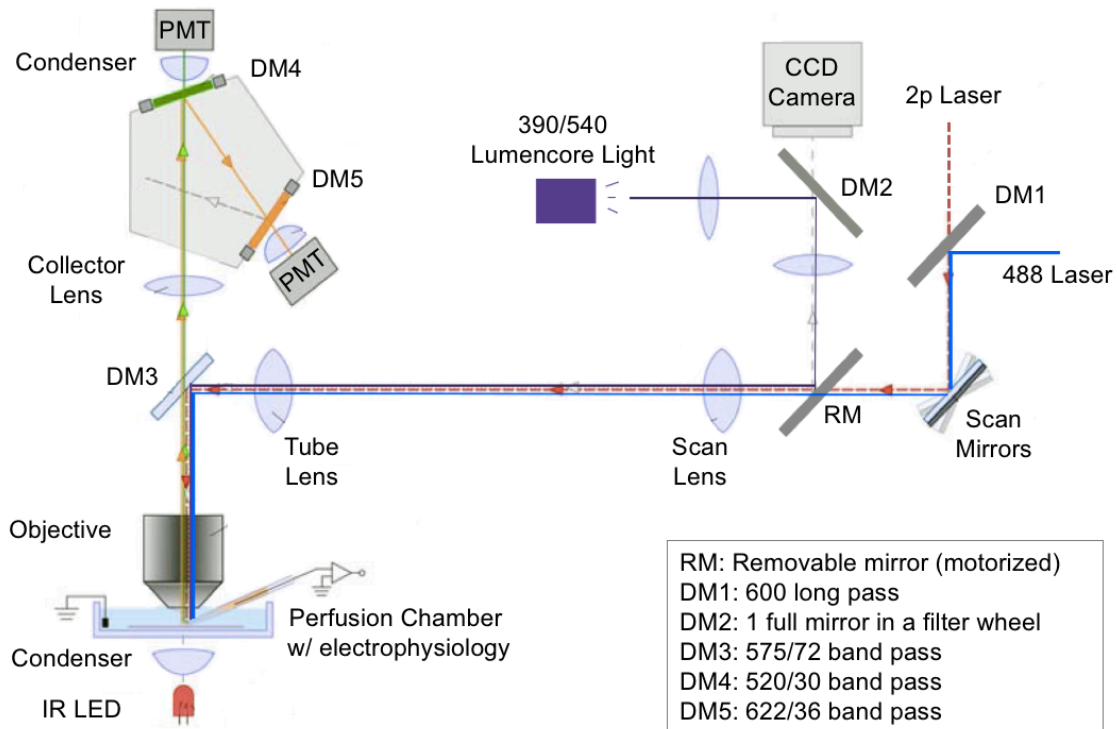
Figure 2.1: Schematic of modified MOM for combined calcium imaging and photo-control. A Moveable Objective Microscope (MOM) from Sutter was modified with a bright light source (Lumencore) for wide-field, whole-dendrite, and background photo-control. It was also modified with a removable mirror (RM) on a motor that was driven by a TTL pulse for protocol automation. Finally, a 488 nm laser (Coherent OBIS) was piped into the microscope via the scan mirrors so that it could be easily targeted to a region of interest. This schematic was modified from (Euler et al. 2009).

During set-up, we co-aligned the 488 nm laser beam with the 2p laser beam, but minute alignment variations from day-to-day offset the two beams by up to as much as 10 μm. We used a two-photon image to outline ROIs for 488 nm laser scanning, so we needed to know this error each day in order to adjust the target ROI appropriately during local VGIC block experiments (see Figure 3.10). To measure the offset at the start of each day, we placed a florescent slide (Chroma) below the objective and defined an ROI (same relative shape/size used for local block experiments). We then scanned with high 488 laser power to photobleach the targeted ROI, imaged the photobleached region again in two-photon mode, and measured the offset between the intended ROI and the actual photobleached ROI (Figure 2.2).
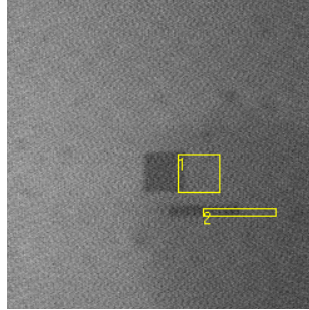
Figure 2.2: Two-photon & 488 beam alignment calibration. Two-photon image of calibration procedure. Displayed is a two-photon image of a florescent slide. Yellow rectangles outline the intended ROI, and darker regions depict the regions actually scanned with the 488 laser. Here, the offset is 10 μm to the left and 1 μm down from the target chosen based on the two-photon image. Subsequent ROI targets for the day were adjusted by 10 and 1 μm in the x and y direction, accordingly.

Experimental Protocols

For ideal calcium recording conditions, we added 100 μM picrotoxin to external solution to block GABAa currents, which will dampen calcium signals (Kanemoto et al. 2011). Picrotoxin is not particularly soluble, so we let the solution mix for at least 30 minutes to ensure picrotoxin powder completely dissolved. To our internal solution, we added 100 μM QAQ, 40 μM Alexa 594, & either 50 μM Fluo-4 (Figure 3.8) or 200 μM Fluo-5f (Figures 3.10, 3.12, 3.14, and 3.15). For experiments measuring somatic action potential generation, experiments were started at least 20 minutes after achieving a whole-cell patch configuration to allow QAQ, Alexa 594 and calcium dye sufficient time to diffuse throughout the cell. Experiments involving dendritic function were started after at least 30 minutes post break-in.

To combine QAQ photo-control with two-photon calcium imaging, we relied on two properties: QAQ is insensitive to 810 nm two-photon light (Figure 3.6), and is bi-stable in the dark with a relaxation constant from *cis* to *trans* of >5 s. QAQ's insensitivity to 810 nm light allowed us to image calcium without photo-isomerizing the molecule. By exploiting QAQ's bi-stability and switching off the photo-isomerization light just prior to imaging, we could avoid high background in the two-photon image due to stimulation light bleeding through the emission filter.

To image one region of interest (ROI) along a dendrite in experiments not involving targeted 488 nm laser light, the entire cell was first illuminated with either 390 or 540 nm light at an optical power density of less than 5 mW/mm^2 to avoid tissue damage and/or physiological effects from light (Yizhar et al. 2011). That light was then switched off and, less than three seconds later, calcium signals were simultaneously evoked by somatic current injection and imaged. This constituted one trial. The photoswitching wavelength was then switched, and the process repeated. We alternated wavelengths between trials and in each trial at least three recordings were acquired for signal averaging. The cell was allowed to recover for 20 seconds after each recording.

For local VGIC block experiments, we first illuminated the whole cell with 390 nm light through the epiflorescent path on the MOM. Then we switched light paths and, for trials with VGIC block, scanned a targeted ROI with 488 nm laser light (< 5 mW/mm^2). No more than

three seconds after the 390 nm light was given, we injected three 2-ms current pulses at the soma to elicit action potentials at 40 Hz, and imaged calcium in the dendrites. We then let the cell recover for 20 seconds. This constituted one trial. With each trial we alternated between *cis* and *trans* conditions, and at least six trials were performed, yielding at least three trials per condition for each ROI. For the weak/strong back-propagating experiments, we illuminated only the dendrites with either 390 or 540 nm light before switching to the scanned light path and imaging calcium. All imaging and photoillumination was coordinated with TTL pulses controlled by the electrophysiology software, pClamp (Axon Instruments).

During the course of an experiment, we took care to use the least amount of light necessary in order to minimize effects on cell-health of direct exposure to UV light, and Alexa 594 photobleaching. Occasionally damaged cells exhibited strong, irreversible plateau potentials with excessive light stimulation. We excluded these cells from our analysis.

2.8 Analysis

Electrophysiology

Input resistance was calculated as the slope of I/V curve close to resting membrane potential. Action potential amplitude was measured from resting membrane potential to peak. In response to a hyper polarizing current step, the sag ratio was calculated as the steady-state voltage divided by the initial sag. Voltage traces with similar steady-state values were chosen to compare across neurons. Synaptic summation was calculated as the ratio of the amplitudes of the last and first EPSP in a train ($EPSP_4/EPSP_1$).

Imaging

Average raw pixel values were extracted from semi-automatically defined ROIs. General regions were first outlined manually in ImageJ, then thresholded in MATLAB. Images were sorted and analyzed with a custom MATLAB program. For each dendritic location, at least three trials were averaged per experimental condition to achieve better signal-to-noise. Calcium transients were quantified as change in calcium florescence (G; fluo-5f dye), normalized by red florescence (R; alexa 594), as follows:

$$dG/R(t) = \frac{G(t) - G_o}{R(t)}$$

Where the baselines (G_o) were taken as an average of the first 500 milliseconds of each trace. All imaging data shown in figures and used for statistical analysis represents peak dG/R values, except for the data in figure 3.8, for which dF/F was used. A measure of calcium using dG/R is more robust to noise because the red florescence signal used for normalization is orders of magnitude stronger than the green calcium florescence. Also, dG/R inherently normalizes for changes in absolute dye amount (different dendritic diameters, etc.), and is relatively insensitive to baseline florescence (Yasuda et al. 2004).

For morphological analysis, we traced neurons using the simple neurite plugin in FIJI (Longair at al. 2011), and performed a sholl analysis to examine dendritic branching patterns, as well as counted the number of primary apical branch points in each cell.

Statistics

For parametric data, values are presented in the text as means ± standard error of the mean, and plotted with error bars representing standard error. Two-tailed unpaired or paired *t* tests were used to evaluate the difference between two group means. For non-parametric data, values are given as medians with bootstrapped 95% confidence intervals, and displayed using box plots (middle line = median; box = 25th and 75th percentiles; whiskers = most extreme data points other than outliers). For non-parametric paired data, we used a Wilcoxon signed rank test, and for non-paired data we used a Wilcoxon rank-sum test. To compare distributions, we used a two-sample Kolmogorov-Smirnov test. The number of cells for each experiment is indicated in the figure legends, or in the text.

3. Results

3.1. Whole-cell photo-control of neurons in acute slice.

QAQ, as an optically-controllable voltage-gated ion channel blocker, has the potential to be a powerful tool to investigate both sub-cellular excitability and voltage-gated ion channels' complex contribution to dendritic computations. In this first section, we introduce QAQ into neurons in acute slice to confirm that its actions on voltage-gated ion channels work as expected in various single-neuron computations.

3.1.1 Photo-control of action potential firing

To confirm previous results on dissociated hippocampal cell cultures (Mourot et al. 2012), we loaded 100 μM QAQ into CA1 pyramidal cells in acute brain. As in dissociated cell cultures, QAQ reversibly regulated action potential firing in CA1 pyramidal neurons in acute slices (Fig. 3.1a).
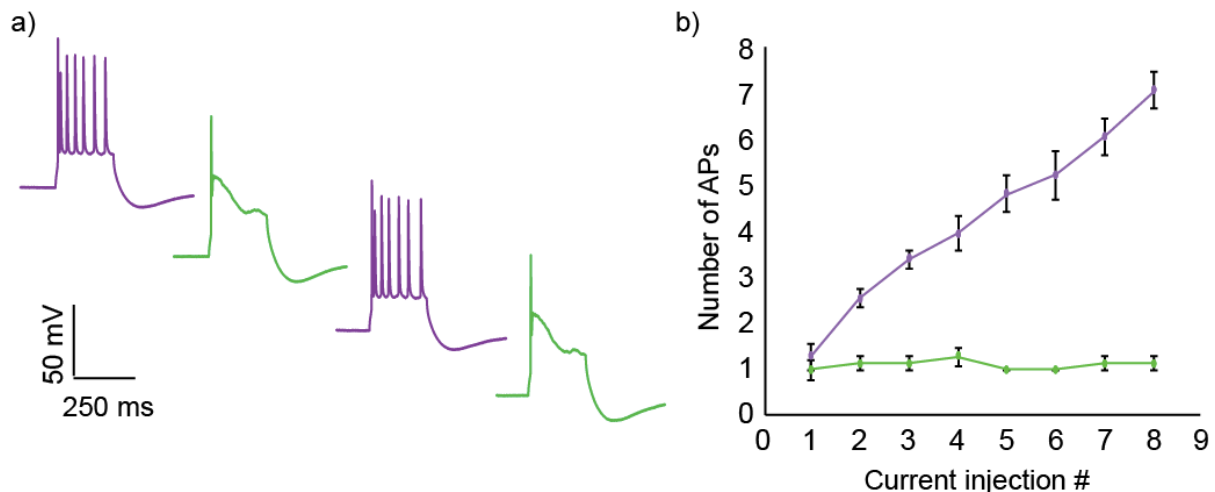
Figure 3.1: Action potential photo-control in CA1 pyramidal neurons. a) Example voltage responses to a 300 pA, 250 ms long current injection at the soma. Control is reversible, as light was switched back and fourth from 390 to 540 nm. b) Increasing current injection amplitudes in 50 pA increments yields increasingly more action potentials in *cis*-QAQ conditions, but only one action potential at all current levels under *trans*-QAQ conditions (p <. 001; n = 7).

In 390 nm light, which converts QAQ to its inert *cis* form, we saw a normal CA1 pyramidal cell step response (Staff et al. 2000). In 390 nm light, cells fired more action potentials with increasing current amplitudes (Fig. 3.1b), and inter-spike intervals increased with subsequent action potentials. When we illuminated cells with 540 nm light to convert QAQ to its VGIC-blocking *trans*-form, cells still fired a first action potential, but repeated

firing was abolished (Fig 3.1a, b). Persistence of the first action potential is likely due to *trans*-QAQ's function as a use-dependent blocker, such that it only blocks channels once they are in the open state (Mourot et al. 2012; Hille 2001). During the first action potential QAQ rapidly blocks the open channels to then abolish subsequent firing. Some photo-control of the first action potential was apparent: action potential amplitude was decreased, and the half-width was increased, as previously noted in cultured hippocampal neurons (Mourot et al. 2012). We also saw an increased after-depolarization (ADP) following the first action potential in 540 nm light (Fig. 3.1a), which was not apparent in dissociated hippocampal cells, but the ADP can be attributed to partial-block of voltage-gated channels (Jensen et al. 1994; Azouz et al. 1996; Metz et al. 2005). QAQ had a similar effect in cerebellar Purkinje neurons (Fig. 3.2), though cells often fired an initial burst of 2-3 spikes at higher current injection amplitudes in these cells, rather than just one initial spike (Fig. 3.2b), which can again be attributed to QAQ's use-dependent nature.
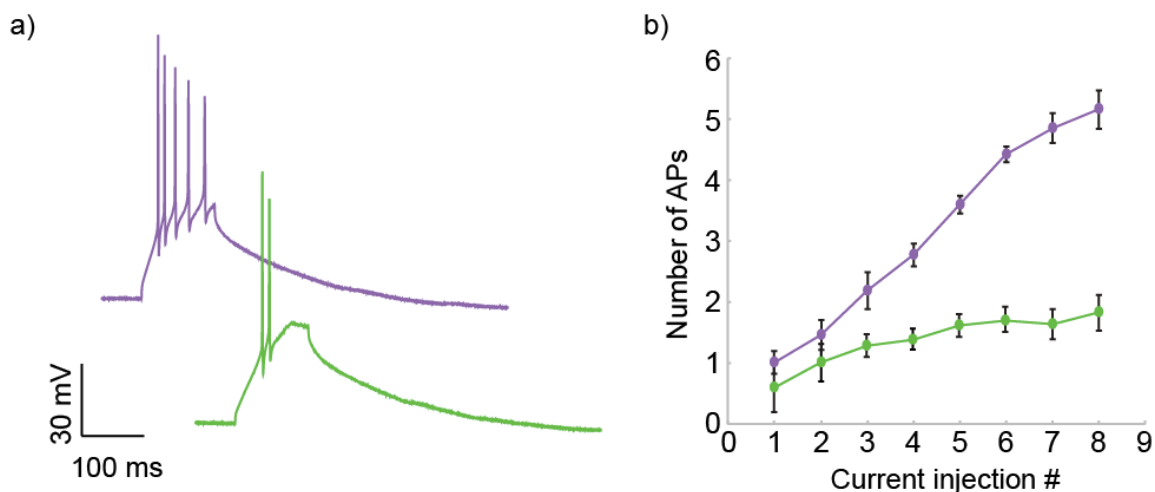
Figure 3.2: Action potential photo-control in cerebellar Purkinje neurons. a) Example voltage responses to a 150 pA, 120 ms long current injection at the soma. Control is reversible, as light was switched back and fourth from 380 to 500 nm. b) Increasing current injection amplitudes by 50 pA increments yields increasingly more action potentials in *cis*-QAQ conditions, but only 1-2 action potentials in *trans*-QAQ conditions (p <. 001; n = 5).

3.1.2 Long-term photoswitching and membrane resistance with intracellular QAQ.

For certain experiments it is necessary to hold a neuronal whole-cell patch for up to 90 minutes. For this thesis research, specifically, to ensure that QAQ has equilibrated throughout the extensive CA1 dendritic tree, experiments on dendritic function didn't even start until 30 minutes after whole-cell break-in (see *Figure 3.7* for a possible equilibration time-course). QAQ's long-term action in a cell has yet to be tested, so we assayed the level of action potential photo-control over the course of an experiment once photo-control had reached steady-state (typically after about 20 minutes of wash-in, though low or high access resistances shortened or lengthened this time). Action potential photo-control was no different at around 90 minutes post break-in than it was just after reaching steady state at

around 20 minutes post-break in (p = .92, n = 11; Wilcoxon sign rank test; Figure 3.3a). During a 250 ms current injection about 150 pA above threshold, the number of action potentials decreased on average from 5 in *cis*-QAQ to 1 in *trans*-QAQ at both time points assayed. We also measured membrane resistance immediately upon break-in (presumably before QAQ had time to diffuse in at all), and at the termination each experiment (excluding terminations due to cell death, or a lost patch), membrane resistance was not significantly different than upon break-in (p = .95; n = 8; Wilcoxon sign rank test; Figure 3.3b).
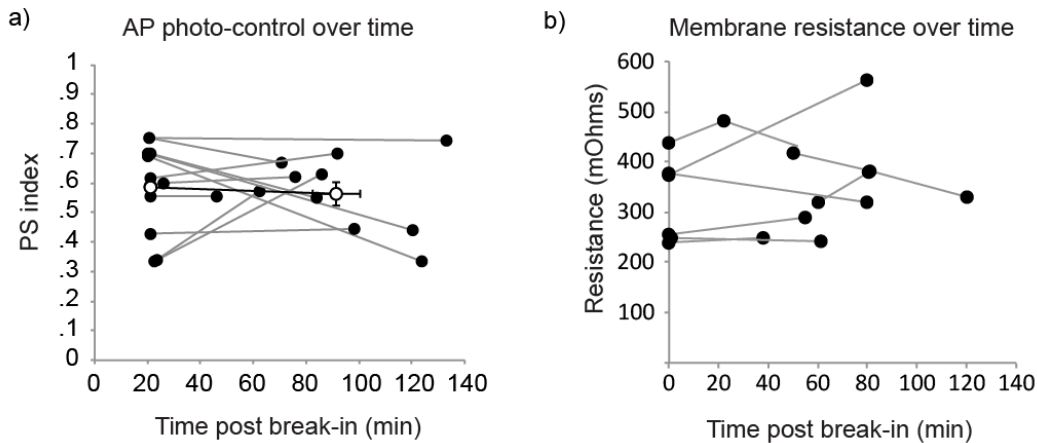
Figure 3.3: Long-term AP photo-control and membrane resistance in whole-cell. a) Action potential photo-control during time in whole-cell, quantified using a "photoswitch (PS) index," which is calculated as $(\#APs_{390} - \#APs_{540})/(\#APs_{390} + \#APs_{540})$. b) Membrane resistance measured upon break-in, and again before the end of each experiment. Neither measure is significantly changed during the course of a long-term recording.

3.1.3 VGIC block enhances EPSP summation in CA1 pyramidal cells.

Previous research has shown that blocking either voltage-gated potassium channels or HCN channels enhances temporal summation in CA1 pyramidal cells (Margulis & Tang 1998; George et al. 2009), but that at the same time voltage-gated sodium and calcium channels can boost sub-threshold EPSPs (J. Magee & Johnston 1995; Lipowsky et al. 1996; Gillessen & Alzheimer 1997). To test the net effect that all VGICs acting together have on EPSPs and temporal summation, we patched CA1 pyramidal cells, let them fill with QAQ (100 μM), then stimulated axons in the *stratum radiatum* to elicit four EPSPs at 50 Hz from Schafer collateral inputs (Fig. 3.4a, b). When we blocked VGICs, single EPSPs were not affected (*p* = 0.08), indicating that VGICs acting together do not boost single EPSPs (Fig. 3.4c). However, we did find that the summation ratio of the fourth to first in a 50 Hz train of four EPSPs was enhanced with VGIC block (Fig. 3.4d), as previous studies have found when blocking voltage-gated potassium channels (Cash & Yuste 1998; Cash & Yuste 1999; Ramakers & Storm 2002). This result indicates that voltage-gated potassium channels, which dampen activity, are the dominant players in this phenomenon.
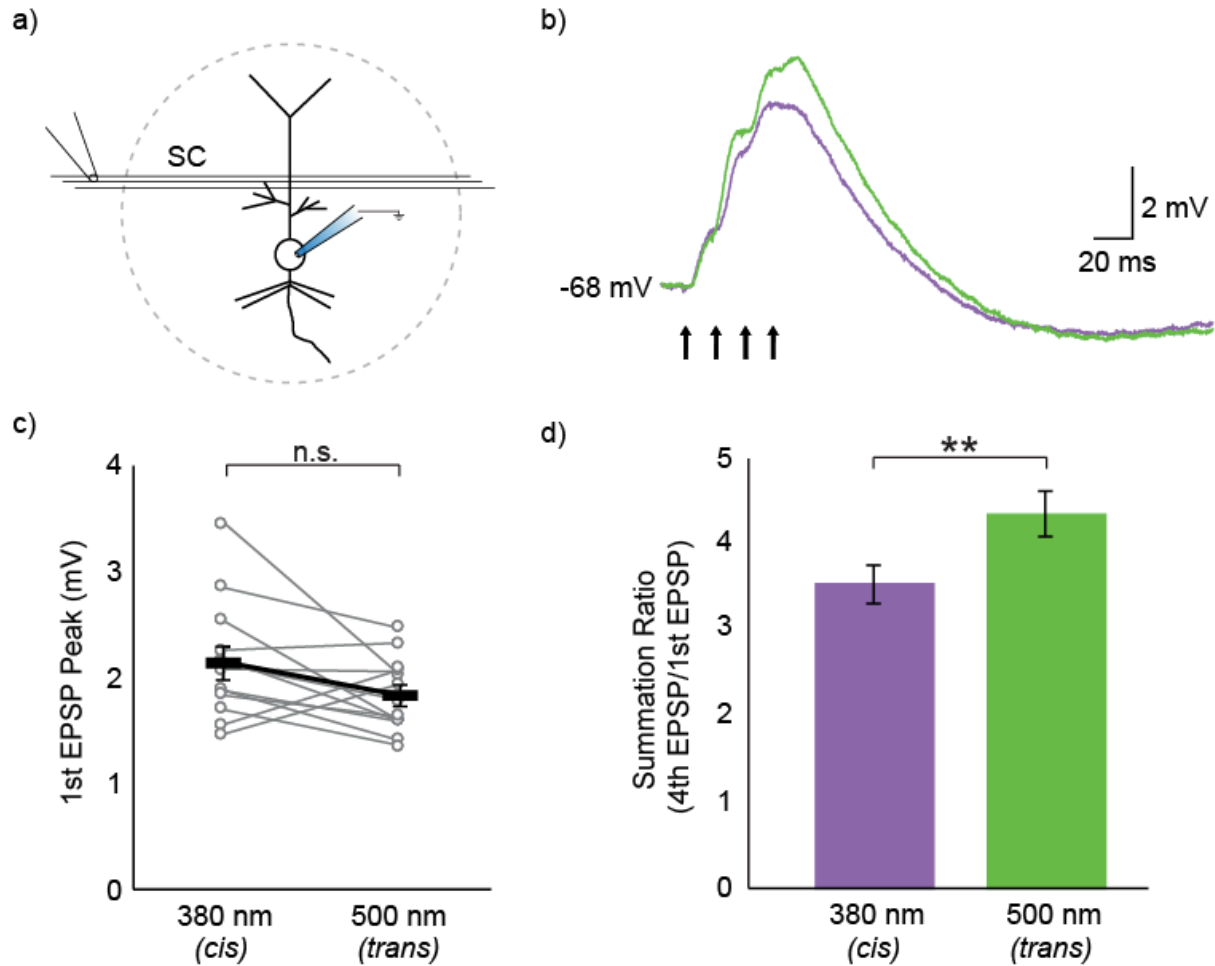
Figure 3.4: VGICs dampen EPSP summation, but do not affect single EPSPs. a) Schafer collateral axons were stimulated to produce EPSPs in the post-synaptic CA1 pyramidal neuron, while illumination light to block or unblock channels was applied to the whole cell. b) Example somatic voltage recording. Four EPSPs were elicited with an extracellular electrode at 50 Hz. c) Blocking VGICs with 500 nm light had no significant effect on the first EPSP peak (p = .08; n = 13; black overlay represents mean ± S.E.). d) The summation ratio of the fourth to the first EPSP peak was enhanced from 3.6 (± .2) with no VGIC block, to 4.4 (± .3) with VGIC block (p = .0081; n = 13). Green signifies 500 nm (*trans*-QAQ) conditions, whereas purple signifies 380nm (*cis*-QAQ) conditions.

Certain voltage gated ion channels have been shown to increase the probability that an EPSP will elicit an action potential, a process termed EPSP-spike coupling (Fricker & Miles 2000; Jester et al. 1995; Daoudal et al. 2002). In light of these results, we expect that blocking all voltage-gated channels in CA1 pyramidal cells will affect EPSP-spike coupling. Because CA1 cells always fire one smaller action potential under *trans*-QAQ conditions (Figure 3.1) we were able to photo-control voltage-gated channels in the whole cell, including the soma, and still measure action potential events. Our results confirm that the voltage-gated channels in CA1 pyramidal cells do indeed enhance EPSP-spike coupling, and that QAQ affects this function, as expected (Figure 3.5).
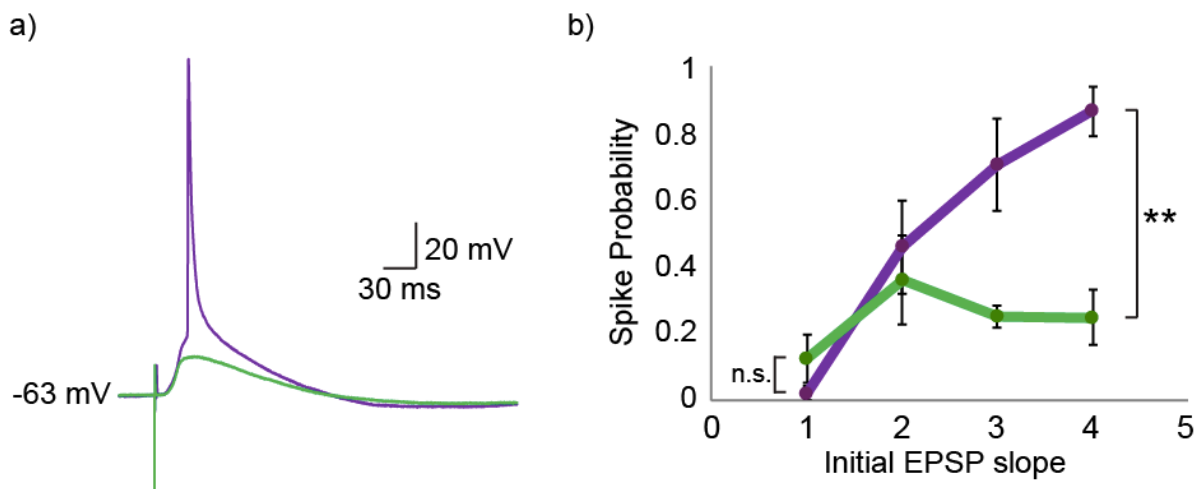
Figure 3.5: VGICs Enhance EPSP-Spike Coupling in CA1 Pyramidal Neurons. a) Example voltage recording in *cis* conditions (purple) and *trans* conditions (green). The stimulation artifact from an extracellular simulating pipette in the perforant pathway marks the time of EPSP simulation. b) Initial EPSP slope was measured over the first 2 ms following the upward inflection point of the EPSP. Spike probability from 3 to 4 mV/ms was significantly greater with VGICs active (purple), than with VGIC blocked (green) (p = .0031), but not for slopes from 1 to 2 mV/ms (p = .76; n = 3 cells).

3.1.4   QAQ two-photon sensitivity.

One way to measure dendritic activity is with florescent calcium imaging (Yasuda et al. 2004). Currently, green calcium indicator dyes are the most effective dyes available for imaging calcium, as red dyes have a tendency to get sequestered in endoplasmic reticulum. These green dyes require one-photon excitation wavelengths in the same spectral range as QAQ, but can also be excited with two-photon wavelengths. In order to use QAQ in conjunction with two-photon calcium imaging for studies described later in this thesis, we needed to know whether QAQ is two-photon sensitive. To test this, we first illuminated with 540 nm light, or 390 nm light to convert the molecule into either its *trans* or *cis* forms, respectively. Then we immediately scanned the soma with two-photon light, using imaging-intensities and acquisition times equal to those we used for later experiments (sections 3.1.5, 3.2.2, 3.3.2, and 3.3.3), and injected a current pulse to assay the step response in each condition (Figure 3.6a, c).

Using a ratio of the integrated step responses (total charge transfer) in *cis* vs *trans* as a sensitive measure of activity, we found no effect of two-photon light on either form of QAQ. When compared to the typical one-photon charge transfer ratio, scanning *cis*-QAQ at any two-photon wavelength between 750 nm and 950 nm had no effect (Figure 3.6b). Similarly, scanning *trans*-QAQ with any two-photon wavelengths between 800 nm and 950 nm was not significantly different than the one-photon charge transfer ratio (Figure 3.6d), also indicating that *trans*-QAQ is unaffected by two-photon imaging light. These results let us perform the imaging experiments covered later in this thesis.

a) Example: no effect of 2p 810 nm light on *cis*-QAQ

390 nm   810 nm   390 nm

40 mV

150 ms

b) Sensitivity of *cis*-QAQ to two-photon light

Charge Transfer Ratio (cis/trans)

2p wavelength (nm)

c) Example: no effect of 2p 850 nm light on *trans*-QAQ

540 nm   850 nm   540 nm

40 mV

150 ms

d) Sensitivity of *trans*-QAQ to two-photon light

Charge Transfer Ratio (cis/trans)

2p wavelength (nm)
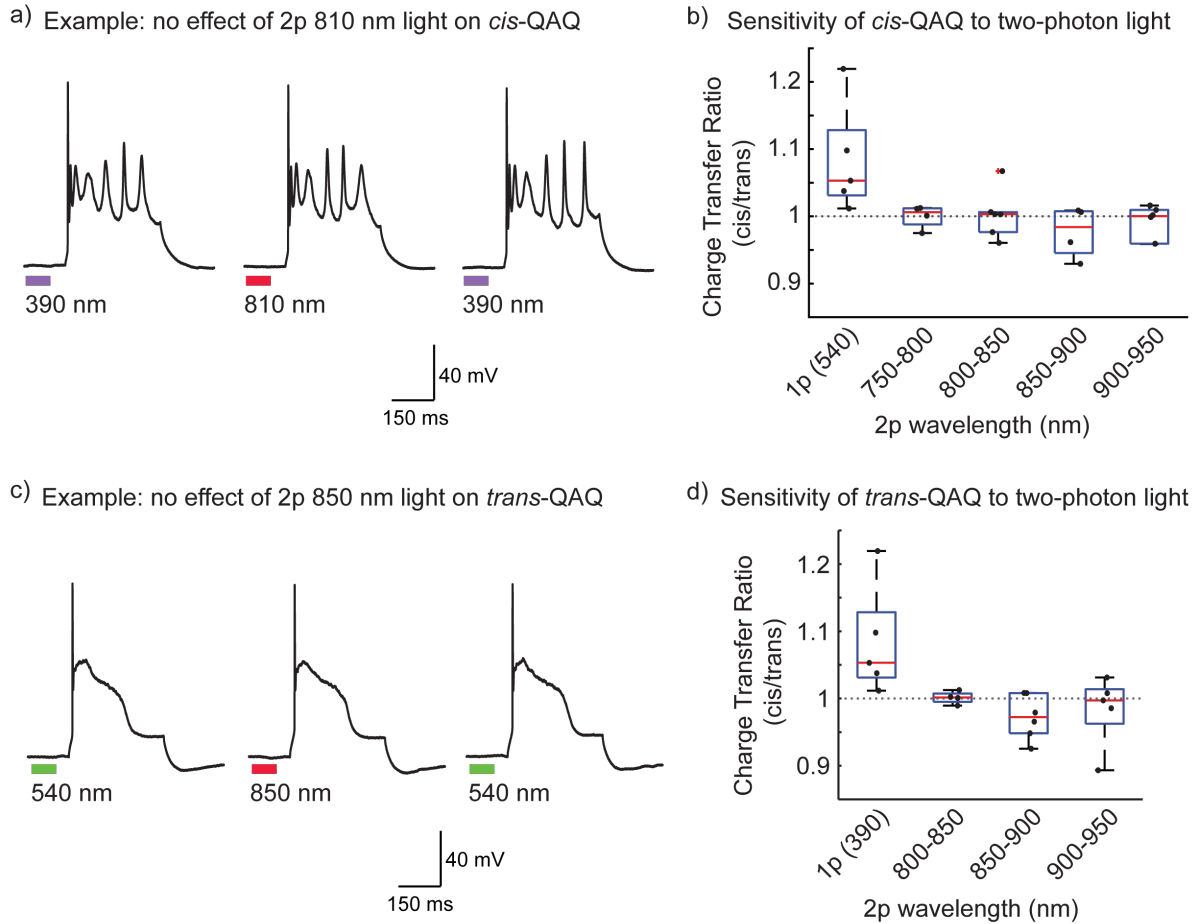
Figure 3.6: QAQ sensitivity to two-photon light. a) Example voltage traces used to determine whether 2p light had any effect on *cis*-QAQ, as measured in CA1 pyramidal cells. A sequence of 390 nm light, then 810 nm 2p light, then 390 nm was given. b) Group data for the ratio of charge transfer in *cis*-QAQ to charge transfer n *trans*-QAQ, binned in 50 nm increments. The initial box represents the one-photon charge transfer ratio for each cell tested, which is significantly greater than all two-photon wavelengths tested (p = 0.032, .030, .016, .0087, respectively). c) Example voltage traces used to determine whether 2p light had any effect on *trans*-QAQ. b) Binned group data for the ratio of charge transfer in *cis*-QAQ to charge transfer in *trans*-QAQ. The one-photon (normal) charge transfer ratio for each cell tested is significantly greater than all two-photon wavelengths tested (p = .032, .0043, .016, respectively).

It is important to note that the step responses seen when testing *cis*-QAQ's two-photon sensitivity (Figure 3.6a) do reflect a slight voltage-gated channel block. Action potentials later in the current pulse are shorter and wider, compared to *cis*-QAQ measurements using just electrophysiology, as above (Figure 3.1). This is due to a 5-second shutter delay between photoisomerization and imaging inherent in our two-photon microscope set-up for these experiments. *Cis*-QAQ slowly relaxes back to it's low-energy *trans* form in darkness with a time constant on the order of seconds, only fully relaxing back after 30 seconds (Mourot et al. 2012). After just 5 seconds in darkness, this slow relaxation is reflected in the step

response. Interestingly, we found that the time course of dark-relaxation speeds up with time in whole-cell (Figure 3.7). This could be because QAQ's diffusion into the dendritic tree is relatively slow, only reaching equilibrium and steady-state dark relaxation kinetics at about 30 minutes post whole-cell break-in (Figure 3.7b). To control for this possibility, all subsequent experiments on dendritic function were performed at least 30 minutes after break-in to let QAQ (100 μM) fully equilibrate in the dendrites.
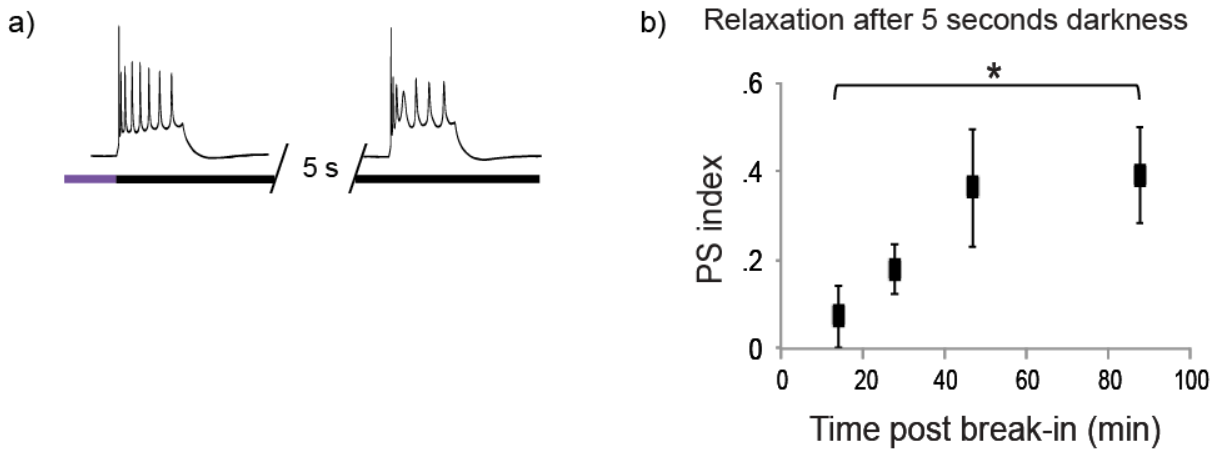
Figure 3.7: Dark-relaxation from cis to trans during time in whole-cell. QAQ has been previously shown to relax from *cis* back to its low-energy *trans* form in darkness with a time constant on the order of seconds. a) Example of the steady-state relaxation is apparent in the step response after 5 seconds in darkness. b) Steady-state relaxation kinetics are not reached until >30 minutes post-break-in. Photoswitch (PS) index is a measure of the difference in mean action potential amplitudes during a step response: (cis-dark)/(cis+dark). Five seconds of dark relaxation yields about a 40% decrease in mean action potential height during a current injection in steady-state. Data is separated into 20-minute bins for display. The initial and final data points before the end of recording for each cell are statistically different (p = .04, n = 8; Wilcoxon sign rank test). Access resistances for each cell remained in a range from 20 to 35 mOhm during each recording.

3.1.5 Photo-control of CA1 dendritic calcium transients.

One important dendritic phenomenon observed in many neuron types, including hippocampal CA1 pyramidal neurons, is an influx of calcium following AP backpropagation (Frick et al., 2003; 2004; Spruston et al., 1995; Stuart et al., 1997). Backpropagating APs (bAPs) can serve as a crucial signal for the induction of synaptic and non-synaptic forms of plasticity, lower the threshold for the generation of dendritic regenerative potentials, or trigger the dendritic release of transmitters/neuromodulators such as endocannabinoids (Bender et al., 2007; Waters et al., 2005).

To gauge QAQ's impact on dendritic calcium influx, we measured Ca^{2+} transients in different locations along CA1 pyramidal cell dendrites with two-photon microscopy. There are challenges in using light both to manipulate and to measure bAP calcium. However, two key properties of QAQ made this experiment feasible. In darkness, *cis*-QAQ is bi-stable with

a relaxation time constant on the order of seconds (Mourot et al. 2012), so that when we switched off photoswitching light, QAQ remained in the same photostate while we then evoked and imaged bAP-Ca^{2+} signals (see *Methods*; Figure 3.8a). We also determined that QAQ is insensitive to 810 nm two-photon imaging light (Fig 3.6), which allowed us to image calcium at those wavelengths without affecting QAQ's photostate.

We found that QAQ decreased bAP-triggered Ca^{2+} transients. Apical dendritic transients were smaller in *trans*-QAQ than in *cis*-QAQ (Figures 3.8b-d). The amount of Ca^{2+} block also increased with distance from the soma (Figures 3.8c-f). QAQ does directly block voltage-gated calcium channels, which likely contributes to the decrease in Ca^{2+} florescence under *trans*-QAQ. But given previous studies indicating that overall calcium channel density remains homogenous throughout the CA1 pyramidal cell dendritic tree (Magee et al 1998, Migliore and Shepherd 2002), we can attribute the progressive increase in calcium signal block along the dendrite to factors other than calcium channel block at each imaging site. This result agrees with previous studies that functional VGICs are necessary for bAPs to propagate normally through the apical dendritic tree of CA1 pyramidal cells.

One caveat of the experiments in section 3.1 is that voltage-gated ion channels were controlled in the entire cell at once. We have confirmed the role of voltage-gated channels in a variety of dendritic functions, confirmed that control is quick and reversible, and confirmed that QAQ does, in fact, control functions previously shown to occur in the dendrites. However, we cannot be absolutely sure that it was the voltage-gated ion channels found specifically in the dendrites that accounted for these results, as previous experimenters cannot be absolutely sure that voltage-gated channels in the dendrites account for specific phenomenon unless they are specifically patch-clamping a dendrite, or locally perfusing channel blockers onto just the dendrites. Particularly in the case of the calcium imaging experiment, it is unclear what contribution both calcium channels directly blocked at the imaging sites, and initial control of action potential generation has on the transient block we report. These concerns, as well as our ability to localize voltage-gated ion channel block will be addressed in the following sections.
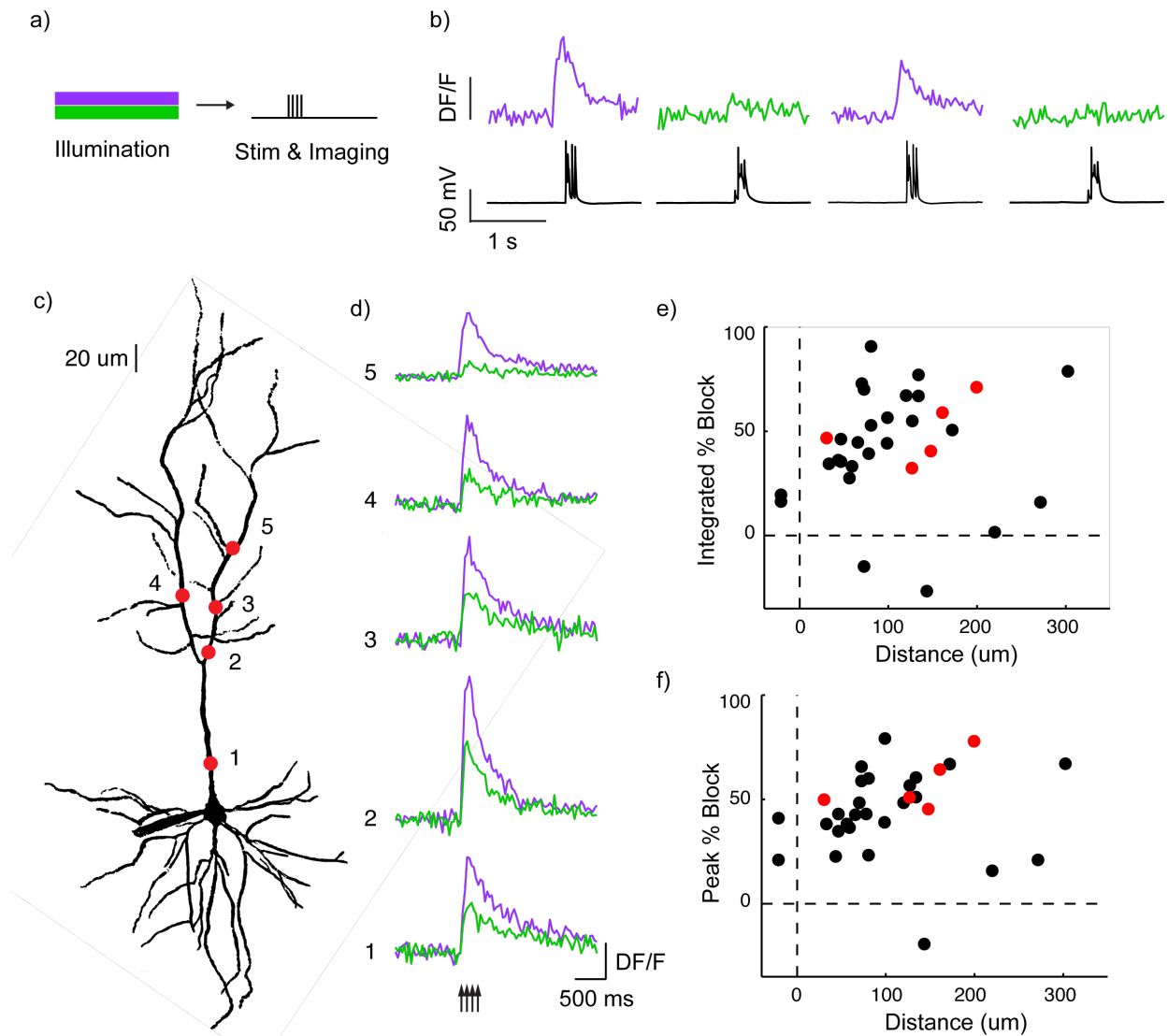
Figure 3.8: Effect of QAQ on bAP-induced dendritic calcium transients. **a**) Experimental protocol. QAQ was photoisomerized by 5 s-long pulses of 380 nm or 500 nm light, followed by immediate stimulation of AP trains (four APs at 25 Hz) via somatic current injections and Ca^{2+} measurements along the apical dendrite. **b**) Four successive bAP-Ca^{2+} traces recorded under alternating light conditions. Corresponding somatic voltage traces are shown below. **c**) Example CA1 pyramidal cell. Imaging regions of interest (ROIs) are indicated by red dots and numbers. **d)** Averaged Ca^{2+} traces recorded at the ROIs shown in (**c**). Purple traces indicate Ca^{2+} transients recorded following 380 nm light pulses, and green traces those recorded following 500 nm light pulses. Each trace is an average of at least six individual traces. **e**) Average of the block of the Ca^{2+} transient integral by *trans*-QAQ as function of distance from the soma. **f**) Average of the block of the Ca^{2+} transient amplitude by *trans*-QAQ as function of distance from the soma. Red dots indicate data points from example cell shown in (**c**) and (**d**). Block is calculated as ($data_{385} - data_{505}$) / $data_{385}$. n = 6 cells.

3.2 Targeting VGIC block to precise spatial regions.

A key advantage of using QAQ to optically control voltage-gated ion channel block is that light can be targeted to small optical regions of tissue, such as sub-cellular dendritic regions. Main parameters that limit the spatial precision to which voltage-gated ion channels can be controlled include: the diffraction limit of light, the point-spread function of the light-delivery system, the light scattering imparted by biological tissue itself, and the fact that QAQ is a freely-diffusible small molecule. The optical diffraction limit represents the physical limit for the degree of spatial localization within which we can photoswitch QAQ. For practical microscopy, this fundamental limit is approximately ½ the wavelength of light, and we will explore the other parameters in this section.

3.2.1. *Laser scattering through CA1 tissue.*

Biological tissue is known to scatter photons (Niemz 2004). In order to determine the limits that our hippocampal slice preparation placed on spatially-targeted light, we made slices of rat hippocampus at varying thicknesses (89-165 µm) and measured the size of targeted laser light spots through these slices.

To be able to block VGICs in a focal region we needed to combine background light for *cis*-QAQ photoconversion with targeted laser light for local *trans* photoconversion. To do so, we used full-field 390 nm light as in section 3.1, and equipped our two-photon imaging microscope with a 488 nm laser (see *Methods*), respectively. QAQ is readily photoisomerized to its trans form with any wavelengths between 480 nm and 550 nm (Fortin et al. 2008). To measure the spot size delivered by a 488 nm laser through hippocampal tissue, we placed each acute slice on top of a florescent slide (Chroma), then focused down through the hippocampus onto the florescent slide (Figure 3.9a). With the 488 nm laser, we then photobleached diffraction-limited spots in the florescent slide underneath various locations within both the CA1 cell body layer (*stratum pyramidale*) or the dendritic layer (*stratum radiatum*), then removed the tissue and then imaged the photobleached spots (Figure 3.9b).

After measuring line profiles through the center of each spot (5-12 spots per thickness and layer; example profiles: Figure 3.9c), we found a significant difference in the half-width of laser light focused through the cell body layer (4.7 ±0.52), vs. through the dendritic layer (2.0 ± 0.22 µm) at tissue thicknesses over 120 µm (p = .002; Figure 3.9d). In general, we found a significantly increased half-width through 89 µm of tissue in the cell body layer (2.3 µm, CI: [1.9, 2.8]) vs. no tissue (1.7 µm, CI: [1.6, 1.8]); p = 0.019; Wilxocon rank sum test), though no significant difference in the dendritic layer at 89 µm tissue thickness (1.6 µm CI: [1.4, 1.9]), compared with no tissue (p = .67; Wilcoxon rank sum test). Focal spot half-width in the dendritic layer is only barely significantly increased at the 165 µm thickness (2.3 µm, CI: [1.9, 2.8]; p = .05). These results tell us that the dendritic layer scatters 488 nm laser light significantly less than the cell body layer, and that photo-control can theoretically be restricted to ~2-3 µm at a cell body near the slice surface, 1.5-2 µm in dendrites near the slice surface, and to 2-3 µm in deeper dendrites.
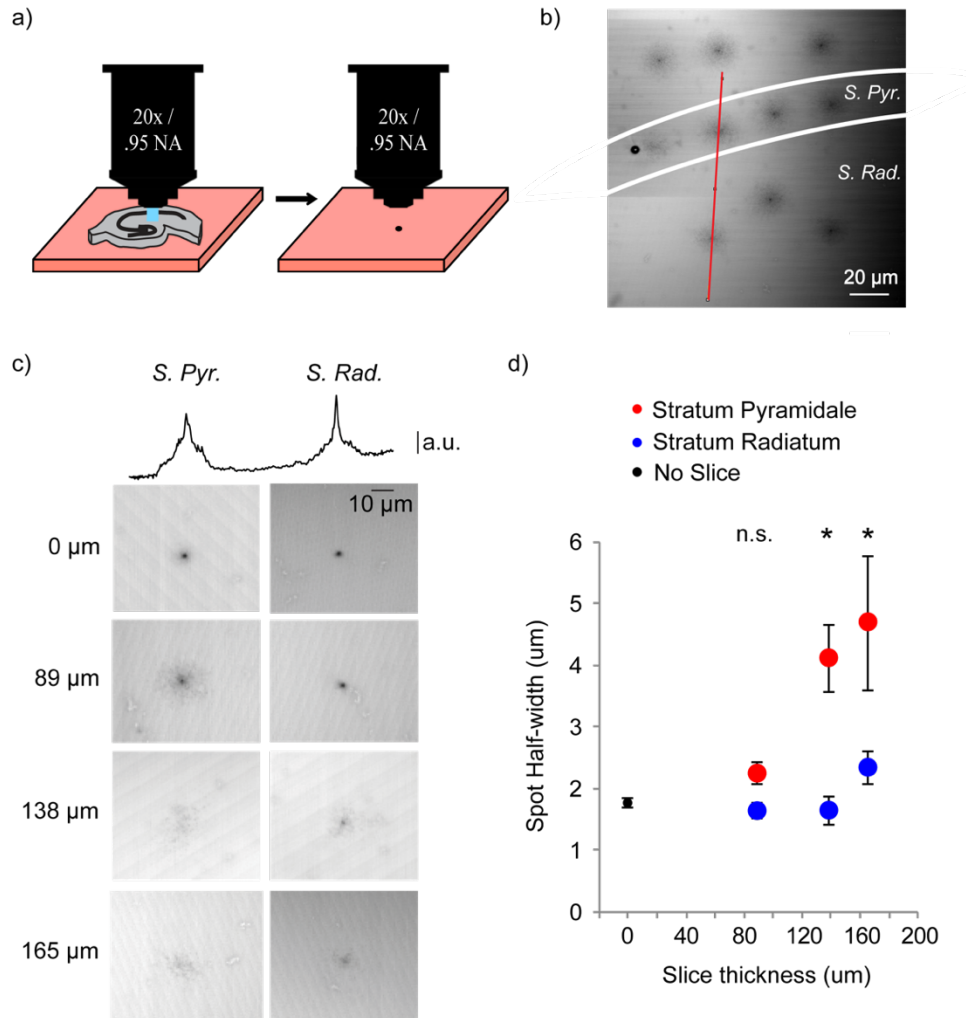
Figure 3.9: Laser scattering through acute hippocampal coronal slices. a) Experimental protocol. An acute slice was placed under a 20x water-immersion objective. Then a 488 laser beam was focused through either the CA1 cell body layer (*Stratum Pyramidale*), or the dendritic layer (*Stratum Radiatum*) to photobleach a variety of focal spots on a florescent slide below. We then removed the slice and imaged the resulting photobleached spots. b) Example two-photon imaging plane following spot-photobleaching through a slice. *Stratum Pyramidale* (*S. Pyr.*) and *Stratum Radiatum* (*S. Rad.*) are marked according to where they were during laser photobleaching. c) Example photobleached spots through each tissue thickness. Top traces are line-profiles through the example spots at 138 μm (arbitrary gray-value units). d) Group data showing significantly broader half-widths through *S. Pyr.* than through *S. Rad.* at thicknesses greater than 120 μm (p <.05).

3.2.2. Local dendritic calcium block.

Because QAQ is a diffusible small molecule, we wanted to know the extent to which its actions can be restricted to a targeted region of dendrite. After confirming that QAQ is not two-photon sensitive (Figure 3.6), we used two-photon calcium imaging to measure local dendritic activity evoked by a train of back-propagating action potentials. To only block

VGICs in a specific region of dendrite, we first illuminated the entire CA1 pyramidal neuron with 390 nm light to globally switch QAQ to its inert *cis* form, then scanned a small (5-20 μm) region of interest (ROI) with a 488 nm laser to photoisomerize QAQ in that region (see *Methods*). Three short somatic current injections at 40 Hz elicited a calcium signal in the dendrites, and we measured florescence changes both within and in the 5 μm immediately next to the targeted ROI (Figure 3.10a, b).
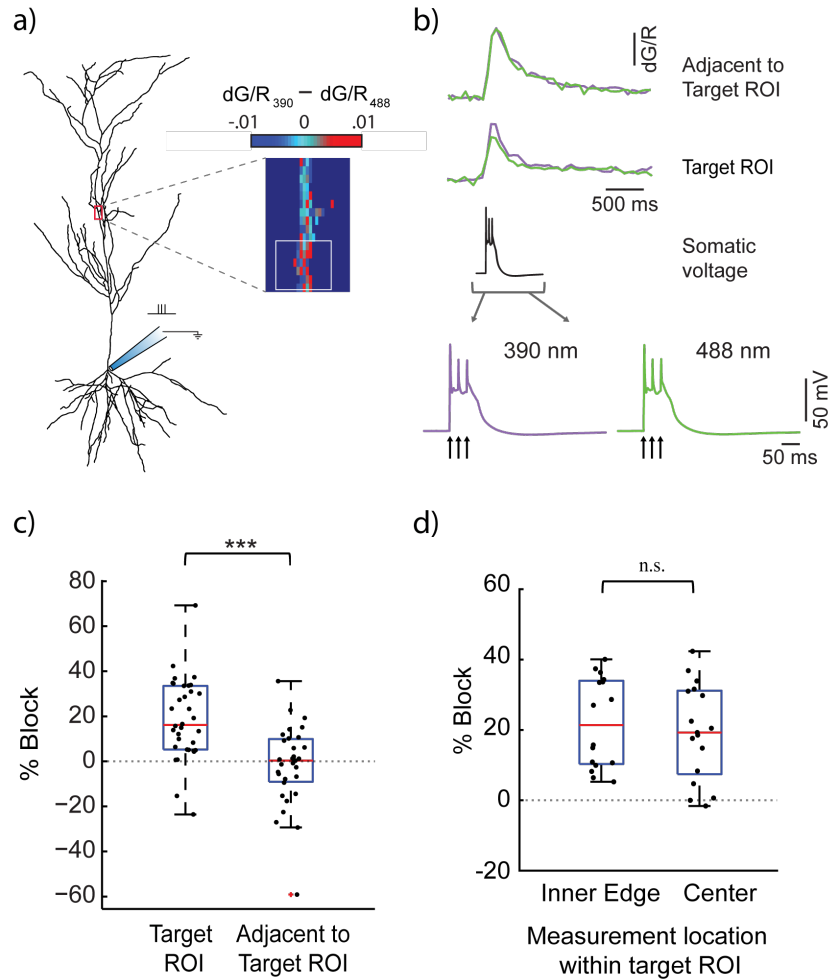
***Figure 3.10: Local dendritic photo-control of bAP calcium transients**. a) Experimental set-up and example ROI image highlighting the difference between peak calcium signals in 390 nm light (*cis*-QAQ) vs. after scanning the targeted ROI (white box) with 488 nm light (*trans*-QAQ). b) Example calcium transients recorded within and next to the target ROI. Green indicates recordings done after targeted 488 laser scanning, and purple indicates recordings done after 390 nm whole-cell illumination. Action potentials were elicited by three brief current injections, and because we always illuminated the whole cell with 390 nm first no difference was seen in voltage at the soma between 488 nm and 390 nm conditions. c) There was a significant difference in the median amount of blocked calcium signal within the target ROI, vs immediately adjacent to the target ROI (p = 2.5415e-08; n = 15 cells, 45 ROIs). d) In a subset of slightly larger ROIs, there was no significant difference in the level of calcium block near the edge (inside 0-3 μm edge) of a target ROI and the level of block in the center (5-8 μm from the edge) of the ROI (p = .602; n = 8 cells, 16 ROIs).*

We found that calcium signal block during a back-propagating action potential is confined to a locally-targeted region (Figure 3.10c). Because the empirical length constant of CA1 pyramidal cell dendrites has been measured to be on the order of 200 to 550 μm (Meyer et al. 1997; Williams 2004), we assumed that any voltage change caused by blocking ion channels in such a small length of dendrite (5-20 μm) is negligible, and that the local calcium block we measured reflects a direct block of local voltage-gated calcium channel activity during back-propagating action potentials. Of data pooled across 13 cells and 28 targeted ROIs, calcium is reduced in a targeted region by 17.6% (CIs: [13.2%, 28.6%]; p = 2.5415e-08, Wilcoxon sign rank test; Figure 3.10b, c), whereas calcium transients in the 5 μm just past the targeted ROI are not significantly affected (0.3% median reduction, CIs: [-5.59, 5.89]; p = .784; Wilcoxon sign rank test; Figure 3.10b, c). This is a relatively small amount of block, considering that QAQ is known to block L-type calcium channels by about 78% and $Ca_v2.2$ channels by about 60% (Mourot et al. 2012). However, many types of voltage-gated calcium channels are present in CA1 dendrites (Lai & Jan 2006), and L-type, N-type, T-type and R-types are all known to be active during back-propagating action potentials (Fisher et al. 1990; Helmchen et al. 1996). QAQ's effect on R and T-type calcium channels remains to be tested, so it is possible that the relatively large level of leftover calcium after local photo-control comes from these ion channels.

In order to test the extent to which diffusion into or out of our targeted photo-control area in the three-second gap between photoswitching and imaging may have affected our measurements, we analyzed calcium block near the edge the target ROI (Figure 3.10d). Previous studies found that calcium diffusion in dendrites is extremely restricted to within 3-5 μm from its source (e.g. a voltage-gated ion channel) (Korkotian & Segal 2006; Biess et al. 2011), so we used this as an analysis guideline. In a subset of target ROIs 10-20 μm long, calcium block within 0-3 μm from the edge of the ROI (21.4%, CI: [10.4%, 33.7%]) was no different from the level of block 5-8 μm from the edge (19.3%, CI: [8.3%, 31.0%]; p = .602). This indicates that diffusion of QAQ (and calcium) at the boundary of a targeted ROI is negligible in the three seconds between photoswitching and imaging, and that photo-control indeed has the potential to be as precise as optically possible (Figure 3.9 addresses this for acute hippocampal slices, specifically).

3.3 Dendrite-specific photo-control of voltage-gated activity.

3.3.1. Dendritic block of VGICs does not affect the somatic step response.

We next tested whether blocking only dendritic VGICs affected the somatic step response. To start, we patched a CA1 pyramidal cell and let QAQ (100 µM) diffuse in for at least 20 minutes. For dendrite-specific photo-control, we restricted illumination light to our field of view (450 µm diameter), then moved a 20x objective over the apical dendrites such that the cell's soma was just out of sight (Figure 3.11a). Because this set-up leaves the soma in the dark, voltage-gated ion channels at the soma were blocked when photo-controlling the dendrites. With somatic illumination, the cell's step response to a current injection was similar to what we saw with whole-cell illumination (Figure 3.1). Firing returned to normal with somatic 390 nm illumination, but blocking VGICs in just the apical dendrites, however, had no effect on the somatic step response (Figure 3.11b). The number of action potentials fired with somatic illumination switched from a median of 5.5 (CI: [3.5, 6.9]) to 1.2 (CI: [1, 3.1]; $p = .002$) with VGIC block, but action potential generation wasn't affected by dendritic illumination ($p = .5$; Figure 3.11c). For a more sensitive measure of whether the somatic step response was affected by dendritic VGIC activity, we looked at total charge transfer in 390 vs. 540 nm dendritic illumination (Figure 3.11d). With somatic illumination, total charge transfer was 7% larger (ratio = 1.07; CI: [1.05, 1.14]; $p = .002$; Wilcoxon rank-sum test) with VGICs unblocked, but with dendritic illumination there was no change in total charge transfer (ratio = 1, CI: [.99, 1.002], $p = .945$; Wilcoxon rank-sum test).
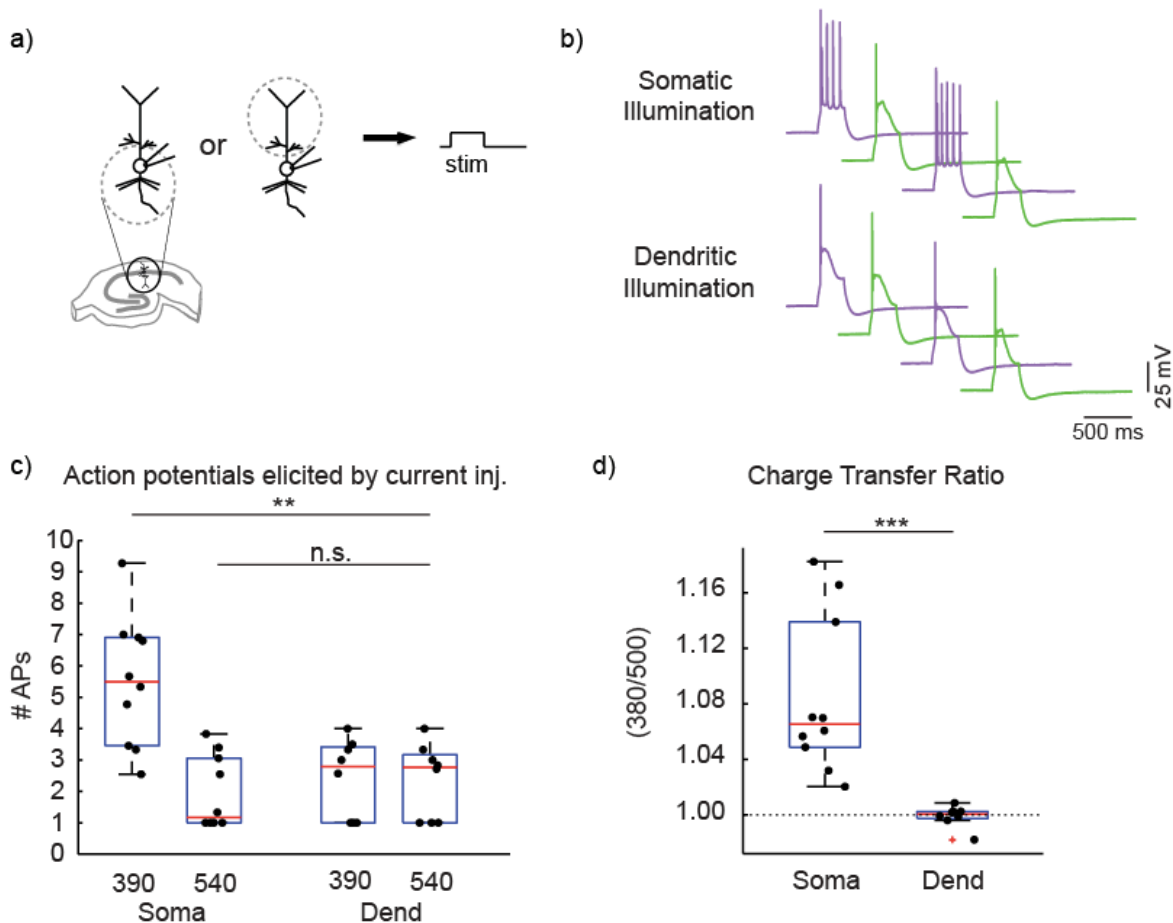
Figure 3.11: Independent photo-control of somatic excitability. a) Experimental set-up. Photoswitching light (gray dotted circle) was positioned either over the soma and axon, or over the apical dendrites, then a 250 ms current pulse was injected. b) Example step responses when VGICs were photo-controlled in the soma, or just in the dendrites. c) The number of action potentials elicited with somatic VGICs unblocked was significantly more than with somatic VGICs blocked, with or without dendritic VGICs blocked ($p < .01$). There was no difference in the number of action potentials evoked with dendritic photo-control ($p > .05$). d) There was a significant effect in the charge transfer ratio of 390 to 540 nm light with somatic photo-control, but not with dendritic photo-control ($p = .00017$).

3.3.2. Localized voltage-gated ion channel function.

Dendritic patch-clamp studies have previously shown that voltage-gated calcium channels along the main apical dendrite are relatively uniformly distributed, though variable from patch-to-patch (J. C. Magee & Johnston 1995; Migliore & Shepherd 2002). QAQ-mediated local block of voltage-gated calcium signals along the dendritic tree confirmed this finding. As in section 3.2.2, we assumed that VGIC block in a dendritic length smaller than 20 µm has a negligible effect on membrane potential and that calcium block is thus a direct measure of localized functional calcium channel activity. We found that the level of local

calcium block was independent of dendritic distance across the dendritic measured range (48 μm to 225 μm; Figure 3.12a), which confirms previous results from dendritic patch-clamping. In addition to the main apical dendrite, we were able to probe oblique dendrites. Due to their small size, oblique dendrites were previously off-limits to local investigation. In the same vein as a relatively uniform main apical dendritic voltage-gated calcium channel distribution, we found that there was also no significant difference between main and oblique local calcium block (Main block: 15.7%, CI: [10.9%, 20.7%], oblique block: 20.4%, CI: [6.5%, 29.2%]; p = .943; Figure 3.12b).

Though we found no general differences in voltage-gated calcium channel function between oblique and main dendrites, it has been proposed that there could exist specific hot spots of excitability along the dendritic tree (Fisher et al. 1990; Wathey et al. 1992; Fitzpatrick et al. 2009). There is also some evidence that L-type calcium channels cluster at branch-points (Shitaka et al. 1996), which could theoretically compensate for jumps in axial resistance that can prompt failure of signal propagation through a branch point (Stuart & Häusser 2007). In light of these ideas, we compared the percent signal block at branch-points to the block measured at least 5 μm away from any branch-point. We found no significant difference between block at branch-points (15.3% block, CI: [8.2, 30.6]) and non-branch points (18.5% block, CI: [10.7, 28.7]; p = .61; n = 13; Figure 12c). Taken together, these results describe a dendritic landscape of voltage-gated calcium current that is generally non-specific for distance from the soma, dendrite type, or branch points, though it is still possible that a small fraction of dendritic regions contain more or less calcium current, and that small fraction is washed out in our population data.
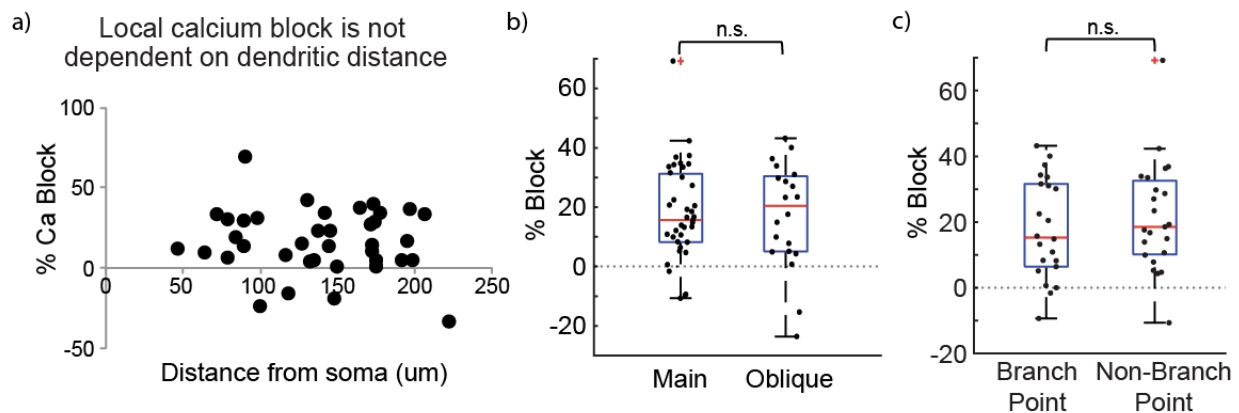
Figure 3.12: Local voltage-gated calcium is relatively uniform across the dendritic arbor. a) Percentage of peak calcium transient block in each 5-20 μm region of dendrite plotted verses distance from the soma. Block was variable, but relatively uniform along the dendrites from 50 to 200 μm from away from the soma (first 50 μm vs. last 50 μm, p = .78; Wilcoxon rank sum test). b) Percentage peak calcium block is no different in oblique dendrites, vs. the main apical dendrite (p = .943; Wilcoxon rank sum test). c) Percentage peak calcium block at a branch point is no different than local block not at a branch point (p = .61).

Using action potential back-propagation as a measure of branch-point calcium activity, we found no differential distribution of calcium current at branch-points vs. not at branch-points (Figure 3.12c). However, signals propagating in the forward direction have a greater propensity to fail solely due to the impedance mismatch of current jumping from a small branch to a larger more proximal dendrite (Stuart & Häusser 2007). Branch-point morphology has also been shown to affect coupling between activity in a branch and that in the soma (Ferrante et al. 2013), indicating that branch-points may be computationally important. It is possible that voltage-gated channels at branch-points also have a specific effect on electrical coupling between branch and soma. To test this, we asked whether locally blocking VGICs at branch-points alters EPSP-spike coupling, a measure of signal propagation efficacy from the dendrites to the soma. To carry out this experiment, we used a double-barrel stimulating pipette so that current flow out of the pipette was local, and then placed the barrel opening 5-20 μm from a visually identified branch in order to stimulate axons impinging on a specific branch (Yasuda et al. 2004) (Figure 3.13a). We then provoked an EPSP, and slowly increased the stimulation amplitude until action potentials were reliably evoked. In three cells, we found no evidence that VGIC block in the 15 μm region around the branch-point of the stimulated dendrite had an effect on EPSP-spike coupling (Figure 3.13b), indicating that VGICs in such a small region at a branch-point do not carry much functional relevance to branch-soma coupling, specifically.
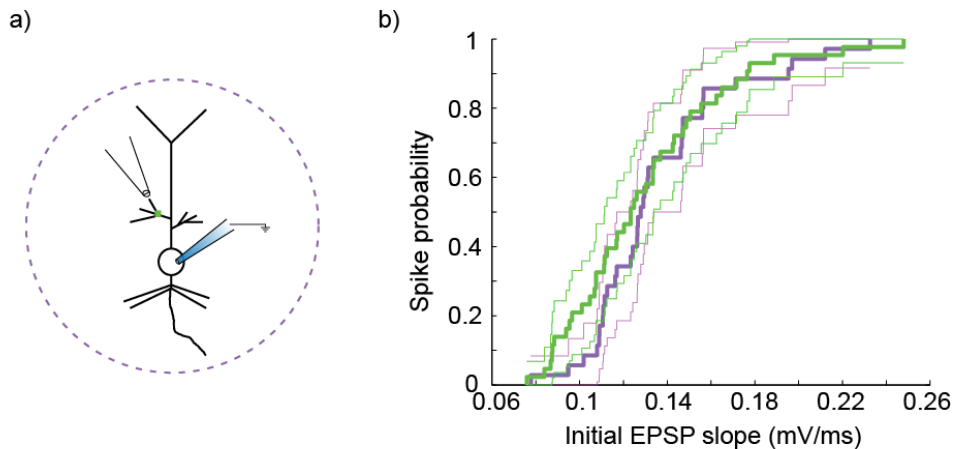
Figure 3.13: Branch-point VGIC block has no effect on EPSP-induced spike probability. a) Experimental set-up. After a cell was filled with Alexa 594 for visualization, a double-barrel pipette was placed near an identified dendrite. Background 390 nm light was used to globally unblock VGICs, and a 488 nm laser was scanned to block VGICs in about a 15 μm region at a branch-point corresponding to the stimulated branch. EPSPs of increasing amplitude were evoked, and ion channel block conditions were alternated during the course of an experiment. b) An empirical cumulative distribution function for spike probability vs. increasing initial EPSP slopes (calculated within the first 2 ms of the initial EPSP upward deflection). Upper and lower 95% confidence intervals are indicated by thin lines. There was no statistically significant difference between VGIC block (green) vs. VGIC unblock (purple; p >.05; Kolmogorov-Smirnov test).

3.3.3   Dendritic VGICs determine strength of action potential back-propagation

Previously, two discrete populations of CA1 pyramidal cells were identified that exhibit either strong or weak dendritic back-propagation (Golding et al. 2001). Modeling suggests that the relative distribution of voltage-gated ion channels along the dendritic tree could account for differences in excitability (Golding et al. 2001; Jarsky et al. 2005; Bernard & Johnston 2003). Here, using dendrite-specific illumination as in figure 3.11, we provide experimental evidence that voltage-gated ion channels do indeed determine the degree of back-propagation.

Because we found that direct block of local calcium in any one area of dendrite is independent of dendritic distance from the soma (Fig 3.12a), we used two-photon calcium imaging to examine the distance-dependent effects of action potential back-propagation. We elicited back-propagating action potentials as in the local block experiments, and alternated whether dendritic voltage-gated ion channels were blocked with 540 nm illumination, or not blocked with 390 nm illumination. In 10 cells, we imaged calcium in at least eight ROIs along the dendritic tree, with the most proximal ("first") and most distal ("last") ROIs separated by at least 100 μm, and identified two discrete populations of action potential back-propagation strength (Figure 3.14a). By examining calcium transients along the dendrite in un-blocked *cis*-QAQ conditions, we labeled cells with propagation efficacies (first 10 μm/last 10 μm) of more than 90% as "strong" propagators (Figure 3.14b), and cells with propagation efficacies less than 60% as "weak" propagators (Figure 3.14c).
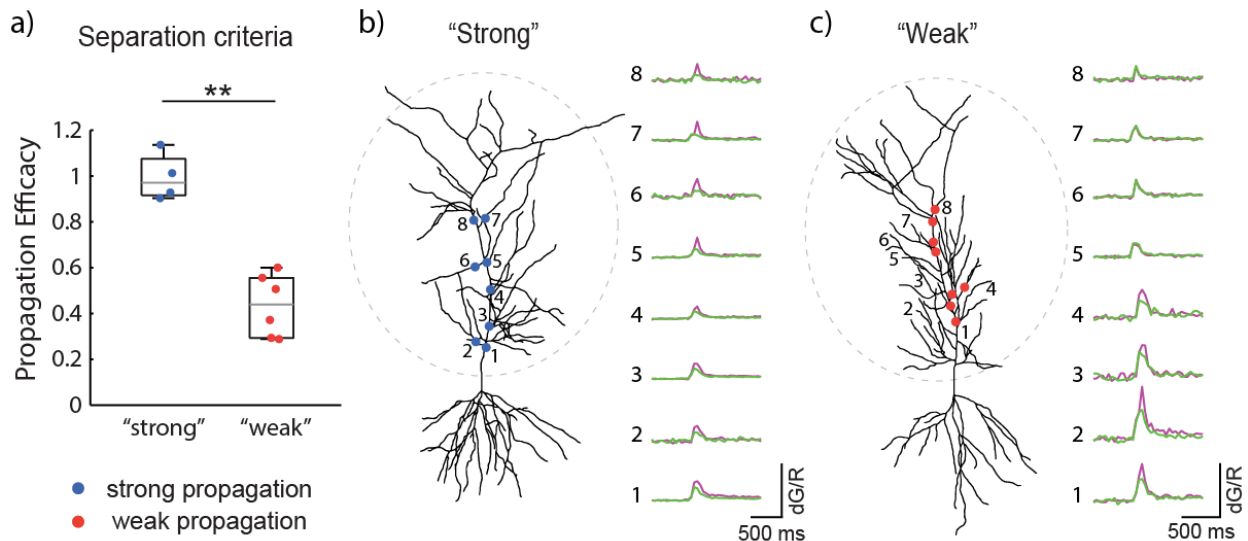
Figure 3.14: Cells exhibited either weak or strong back-propagation. a) Cells were separated into "weak" or "strong" propagators based on their propagation efficacy in unblocked conditions (*cis*-QAQ), as measured from the most proximal ROI to the most distal ROI (Ca_{prox}/Ca_{dist}). Cells with less than 60% propagation efficacy were classified as weak, and cells with more than 90% classification efficacy were classified as strong. b) Example of a strongly back-propagating neuron. c) Example of a weakly back-propagating neuron. Green traces represent VGIC block with dendrite-specific 540 nm illumination, and purple traces represent VGIC unblock with 390 nm dendritic illumination. In both b) and c), calcium traces are equal in scale, and numbered dots indicate the measurement location of each corresponding calcium transient.

To compare the two populations, we pooled all data from strong cells and all data from weak cells into two groups, then binned the data in 40 μm increments for analysis. The weak propagating group showed a significant decay to 36% (± 8%; p = .0029) of the initial calcium level by the farthest distance measured, whereas the strong group showed no significant decay from the initial calcium level over all distances measured (p = .2; Wilcoxon rank sum test; Figure 3.15ai). The relative calcium between the two groups was already significantly different 40 μm away from the initial bin (weak = 77% ± 5%; strong = 99% ± 6%; p = .011; Wilcoxon rank sum test; Figure 3.15ai). When we then blocked dendritic voltage-gated ion channels, there was no longer a significant difference in relative calcium decay between the two groups, except for a barely significant difference still evident at the farthest region from the soma (weak = 64% ±14%, strong = 120% ± 24%; p = .046, Wilcoxon rank sum test; Figure 3.15aii).

Interestingly, when we looked at the absolute calcium levels between the two groups in unblocked, 390 nm conditions, the weak propagators actually showed a significantly higher initial calcium level (dG/R = .055 ± .006) than the strong propagating group (dG/R = .023 ± 002; p = .00077). However, this level decayed rapidly to become even with the strong group at distances greater than 150 μm from the soma (Figure 3.15b). The absolute calcium level in the strong propagating group remained moderate and consistent along the length of dendrite measured.

When we looked at the effects of dendritic voltage-gated ion channel block on absolute calcium signals, we found strikingly different effects on each group. At distances closer than 100 μm to the soma, the weak group (Figure 3.15ci) displayed a greater amount of signal block (35.6% ± 2.9%) than the strong group (Figure 3.15cii, d; 16.1% ± 3.6%; p = .00038). However, with increasing distance from the soma, signal block in the weak group decreased sharply to just 0.8% (± 4.2%) beyond 190 μm (p = 8.68e-07 compared with proximal signal), but block in the strong group actually increased slightly to 27.4% (± 6.3%) beyond 190 μm from the soma. Though this was not significantly different than the proximal block in the strong group (p = .18), it was significantly greater than the amount of block past 190 μm in the weak group (p = .002). This indicates that voltage-gated ion channels had little effect on back-propagation farther from the soma in the dendrites of weak cells, but significantly boosted signals in farther regions of strong cells.
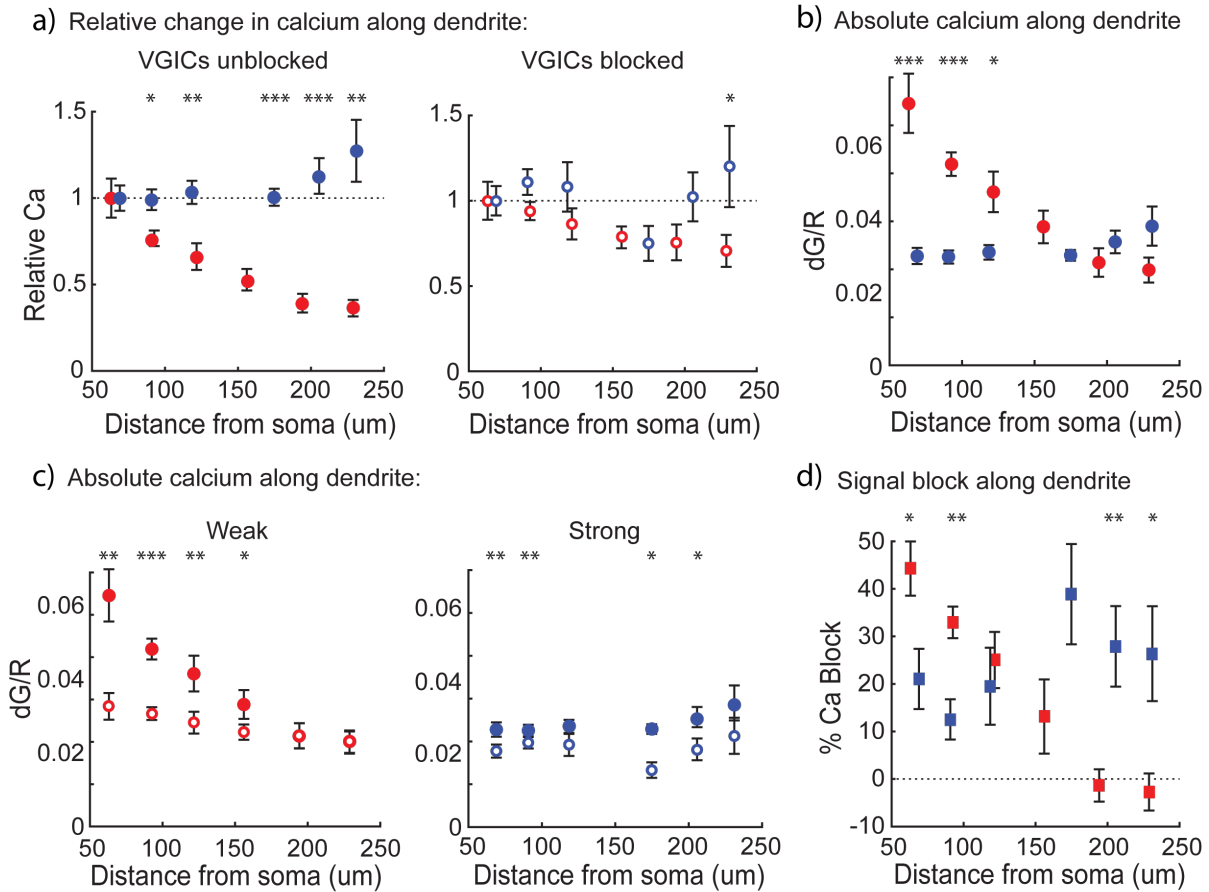
Figure 3.15: Dendritic VGICs determine back-propagation strength. All data from strong cells, and all data from weak cells was binned in 40 μm increments to compare two groups. a) Relative to the first bin, normal propagation (unblocked VGICs) in the weak group significantly deviates from the strong group in all bins after the first (p = 0.91, 0.011, 0.0032, 0.00026, .000046, 0.0025, with respect to dendritic distance). With VGIC blocked, however, there is no significant difference between the two groups, except for a mild effect still apparent at the most distal bin (p = 0.97, 0.087, 0.30, 0.68, 0.10, 0.046, respectively). b) In the weak group, absolute calcium transients were significantly larger at proximal regions than in the strong group, but no different in more distal regions (p = 0.00077, .0000043, 0.035, 0.71, 0.32, 0.14, respectively). c) Calcium transients in the weak group were significantly reduced by blocking VGICs in only more proximal regions (p = 0.0020, 5.39e-07, 0.0014, 0.041, 0.38, 0.55, respectively), whereas calcium transients in the strong group were significantly reduced with VGIC block in both proximal and distal regions (p = 0.0098, 0.0085, 0.064, 0.023, 0.020, 0.13, respectively). d) Comparing the effect of VGIC block on the amount of signal reduction across groups, we see that in proximal regions VGIC block in the weak group caused a greater level of block than in the strong group, but at more distal regions, signal block in the strong group was greater than in the weak group (p = 0.011, 0.0024, 0.52, 0.076, 0.0062, 0.038, respectively). For within group comparisons, p values were calculated using the Wilcoxon signed rank test. For strong v. weak comparisons, p values were calculated with the Wilcoxon rank sum test.

Modeling work has shown that differences in morphology can substantially affect back-propagation characteristics (Vetter et al. 2001). For this reason, we analyzed the morphology of cells in both strong and weak groups. A sholl analysis of dendritic complexity (Sholl 1953) revealed no difference in the dendritic branching pattern between strong and weak propagating cells (Fig 3.16a). There was also no difference in the number of primary branches off of the main apical dendrite between the first and last imaging ROI for each cell (Fig 3.16b). These results indicate that dendritic branching patterns were not responsible for the differences in back-propagation we saw, and further implicate a balance of dendritic VGIC populations in each cell as the underling factor in back-propagation differences.
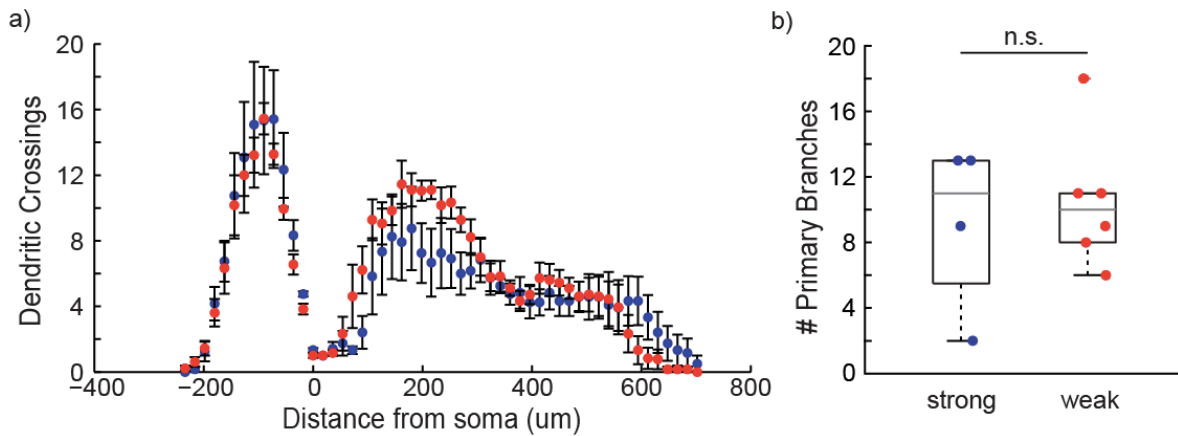
Figure 3.16: Dendritic morphology does not differ between strong and weak groups. a) Sholl analysis of dendritic complexity. The dendritic branching pattern between weak (red) and strong (blue) neurons is not significantly different (p = .72; Two-sample Kolmogorov-Smirnov test). b) Numbers of primary dendritic branches between the most proximal and distal ROIs in each cell did not differ between strong and weak groups (p = .97; Wilxocon rank sum test).

4. Discussion

4.1. Conclusions & new hypotheses

Here we offer new experimental evidence that dendritic VGICs underlie the distinction between weak and strong action potential back-propagation, a notion that has previously only been simulated (Golding et al. 2001; Bernard & Johnston 2003). We identified two populations of CA1 pyramidal cells that display either weak or strong back-propagation characteristics. Weakly propagating cells exhibited a large calcium signal in the apical dendrites proximal to the soma, but a dramatic signal fall-off with dendritic distance, and strongly propagating cells exhibited a moderate calcium response initially that remained stable along the apical dendrites. When we blocked VGICs, weak and strong cells were suddenly indistinguishable. Using percent calcium block in this situation as a measure of absolute excitability, we found that weak and strong populations displayed two different excitability profiles. The weak propagators contained a steep excitability gradient that decreased with distance, whereas strong propagators had a mild excitability gradient that increased with dendritic distance.

Back-propagating action potentials are thought to serve as a signal of recent neural output to dendrites and synapses. Back-propagation can both strengthen or weaken synapses based on recent synaptic input (Markram et al. 1997; Magee & Johnston 1997), and can increase the local intrinsic excitability of a recently-activated dendritic region (Frick et al. 2004). It has also been discovered that hippocampal neurons are differentially-tuned, such that some respond broadly to a variety of input patterns, whereas others respond only occasionally to very specific input patterns (Petersen & Crochet 2013). We hypothesize that the stark contrast in excitability profiles of weak and strong neurons might differentially affect each population's response properties and input coding rules. It is possible that the mildly increasing excitability gradient in the strong population, which produces a "normalized" calcium level along the dendritic tree, serves to potentiate near-by synapses to similar degrees during activity, leading to less dendritic compartmentalization, and more generalized responses to varied input patterns—a broadly-tuned cell. Contrary to this, the steep excitability gradient in weak cells produces a large difference in the calcium levels along the dendrites, which would have very different plastic effects on each active synapse. We hypothesize that this may promote more compartmentalized dendrites, and a cell that learns to respond to only specific patterns of input—a sharply-tuned neuron. Voltage-gated ion channel control of weak and strong back-propagation may alternatively be a consequence of the specific tuning properties of a cell, or genetically pre-determined. Future studies could address these questions.

In a separate experiment we found that dendritic VGICs as a whole suppress EPSP summation, which supports previous studies indicating potassium channels are the dominant players in EPSP summation. HCN channels have also been heavily implicated in CA1 pyramidal cell temporal summation, however, QAQ has been shown to not affect HCN channels (Mourot et al. 2012). It's been theoretically proposed that HCN channel activity alone is too simple an explanation to explain the temporal summation regulation (Desjardins et al. 2003), so it's possible that both HCN and voltage-gated potassium channels have independent but similar effects on summation, and indeed, there is evidence for this idea (George et al. 2009). Additionally, one should keep in mind that full dose-response profiles

for all channels that QAQ acts on have not been measured, but QAQ has so far been shown to affect the same channels as the drug from which it was derived, QX-314 (Mourot et al. 2012), and at high concentrations, QX-314 has been shown to block CA1 pyramidal cell sag current during a hyperpolarizing current step (Perkins & Wong 1995), so it is possible that QAQ does actually have a minor affect on HCN current in CA1 pyramidal cells, though previous experiments in dissociated trigeminal neurons did not find any effect of QAQ on HCN current directly.

When we specifically targeted illumination light to the apical dendrites to block VGICs there, we found no effect on the somatic step response in measures of either action potential firing or charge transfer. This is an important finding because small changes in dendritic properties have been shown to affect action potential firing (Magee & Carruth 1999; Eyal et al. 2014). This experiment also informs our back-propagating action potentials results, in that we can be confident that the difference in propagation we see with dendritic VGIC block is not due to an effect on initial action potential firing.

We also found that local block of back-propagating calcium activity is confined to a target area, and the amount of block is not dependent on distance from the soma. This was also an important finding to support our back-propagating results, because we could be confident that the propagation effects we measured with calcium imaging were not due to distance-dependent changes in localized calcium block at each imaged region. Our analysis of local calcium block supports previous research (Korkotian & Segal 2006; Biess et al. 2011) that calcium diffusion from a source (i.e. voltage-gated calcium channels) is extremely restricted to within a few microns, and demonstrates that diffusional blurring of QAQ's action boundaries is negligible over the course of just three seconds.

Interestingly, we found no difference in the amount of calcium signal blocked in oblique branches compared with the main apical trunk. Previous research has shown that oblique dendrites may be more excitable than the main dendrite (Losonczy & Magee 2006; Migliore et al. 2005; Frick et al. 2003), but we found no differences in the level of local calcium block between these regions. Any excitability differences may then arise primarily from differential voltage-gated sodium and potassium channel distributions. Using QAQ block of activity as a measure of voltage-gated excitability, it would be interesting in future studies to examine how levels of branch excitability correlate with input tuning properties or with EPSP-spike coupling.

In this study, we present the first experimental evidence that VIGCs underlie cell-to-cell differences in action potential back-propagation. Using a method that is more easily tractable than dendritic patch-clamp recordings and amenable to thin dendrites, we also confirm previous electrophysiological and immunolabeling evidence that the general distribution of voltage-gated calcium channels is relatively uniform along the apical dendritic tree. We also add that voltage-gated calcium activity is no different between main and oblique dendrites. By blocking all voltage-gated ion channels to essentially make the dendritic tree passive, we present definitive evidence that schaffer collateral EPSP summation is suppressed by the VGICs in CA1 hippocampal pyramidal cell dendrites. This suggests that, indeed, potassium channels are dominant players in sub-threshold temporal summation, because if sodium and calcium channels played a dominant role, then blocking all VGICs would yield an opposite effect on summation.

3.2. Considerations for using QAQ

QAQ can potentially address a wealth of open questions about voltage-gated information processing in dendrites, but there are, of course, drawbacks to using light to manipulate neural activity. One main complication is that too much light can damage tissue (Niemz 2004). Brain tissue absorbs UV light particularly well (Yaroslavsky et al. 2002), so care should always be taken to measure light output and avoid inundating a cell with more power than is safe. QAQ is readily photoisomerizable with short 300 ms pulses of light at power densities between 1-10 mW/mm^2, which is well below the safe upper limit for brain tissue of 75 mW/mm^2 with short (<500 ms) pulses (Cardin et al. 2010).

It should also be noted that QAQ is a use-dependent ion channel blocker, meaning that it's action will get stronger with repeated activity. It has been noted that at concentrations higher than 200 μM, QAQ will block open ion channels faster and may eliminate even the first action potential during a step response (Fedorchak et al, *in preparation*), but higher concentrations than 200 μM do not allow for complete recovery of action potential firing in *cis*-QAQ illumination conditions. The lack of return to a normal firing pattern at high concentrations is attributable to the fact that QAQ photoisomerization is only about 90% efficient (Fortin et al. 2008). This means that even when we illuminate with near-uv light to convert QAQ to its inert *cis* form, there is still about 10% *trans*-QAQ present. At lower concentrations, this proportion of residual-*trans* is not enough to block channels and disrupt the cell's normal firing pattern, but at higher concentrations, the residual-*trans* in near-uv light is enough to keep ion channels partially blocked. Higher concentrations of QAQ may, however, equilibrate faster in the dendrites and allow dark relaxation kinetics to reach steady-state faster, but this remains to be tested.

QAQ is non-specific for all voltage-gated ion channels tested so far, but there are many others that have not been tested. For the tool to be as useful as possible, it will be critical to both measure full dose-response curves for the ion channels already tested, as well as other channels. It's possible that at certain concentrations, QAQ may be able to tease out contributions from specific ion channels.

Researchers may be tempted to combine QAQ with other optical methods to control neural activity, like glutamate uncaging or optogenetic activation. It is certainly possible to multiplex optical methods, as we have multiplexed calcium imaging and voltage-gated photo-control in this thesis. However, careful attention should be paid to any overlap in spectral sensitivities for each tool. The visible light wavelengths used to photoisomerize QAQ are also known to uncage neurotransmitters, and to affect the channel conducting state of popular opsins (Bamann et al. 2008). Red-shifted versions of QAQ could mitigate these potential barriers in the future, but careful experimental design will be critical for such studies. To effectively combine methods with overlapping spectra, for instance in the case of microbial opsins, we propose that one could tune the light intensity used for opsin activiation in order to offset the change in opsin conductance after 390 or 500 nm illumination. Alternatively, if an experiment allows, light may be targeted to different spatial areas to avoid cross-talk completely.

3.3. Future directions

An optical revolution has opened up new experimental avenues in neuroscience, and we demonstrate in this thesis that the specific photoswitch, QAQ, is a unique and useful tool for previously unattainable studies on dendritic excitability. We anticipate that with the

technical knowledge presented here, one could preferentially control voltage-gated excitability in single dendritic branches, or even spines, and study—for the first time—the functional implications of local VGIC populations in a dendritic tree.

We also demonstrate in this thesis that EPSP-spike coupling is reduced with whole-cell VGIC block, but not with block targeted to a specific branch-point. One open question is whether VGIC block in a whole dendritic branch will affect EPSP-spike coupling, or whether block closer to the soma might have a larger effect. Does branch excitability drive EPSP-spike coupling? Similarly, does branch excitability determine temporal integration, or is this controlled along the entire dendritic tree as EPSPs propagate to the soma? It's been shown that clustered synaptic inputs on a single dendritic branch can evoke an NMDA-based dendritic spike, but that distributed inputs summate linearly at the soma (Yang et al. 2014). Will clustered inputs drive NMDA spikes without voltage-gated ion channel activity? Will passive dendrites yield sub-linear summation of distributed inputs?

We found in this thesis that QAQ's action can be extremely spatially restricted in a dendrite. It will be interesting to examine what effect, if any, VGICs have in the tiniest dendritic regions: spines. VGICs are found in spines (Trimmer & Rhodes 2004; Bloodgood & Sabatini 2007; Tippens et al. 2008), but their purpose there is entirely unclear. Because spines are such electrically compact compartments, even a small number of voltage-gated ion channels could powerfully affect membrane potential. By focally blocking (or unblocking) spine VGICs, one could ask whether they control bAP invasion into spines (Palmer & Stuart 2009), whether they modulate sub-threshold EPSPs or calcium dynamics, or whether VGICs affect changes in spine morphology at all.

QAQ is non-specific for a variety of voltage-gated ion channels, so it will be best put to use for questions concerning general voltage-gated excitability governed by all the channels in membrane. However, if one wanted to use its optical specificity to tease out the specific contributions of certain channels, QAQ could be combined with traditional pharmacological tools.

Finally, QAQ does not cross lipid membranes, but if one wanted to use QAQ for more systems-level questions about branch-excitability, previous research has shown that it can enter cells through pore-dilating TRPV1 or P2X channels. We foresee that it would be possible to exogenously express TRPV1 in a specific population, then apply QAQ with a pore-dilating agonist like capsasin to load it into a whole population. Depending on cell-type, there should be little-to-no occurrences of off-target loading into cells with endogenous TRPV1, as these channels are rare in the central nervous system (Cavanaugh et al. 2011; Arenkiel et al. 2008), and could even be knocked out first if desired (Birder et al. 2002).

Dendritic spikes in the apical tuft of pyramidal neurons have been shown to correlate with behavior, though studies also confirm that activity in the tuft does not propagate reliably to the soma in-vivo. With such a TRPV1/capsasin/QAQ system, one may differentially "turn on and off" voltage-gated excitability in a tuft, and directly ask what effect this manipulation has on behavior. Recently, dendritic calcium transients have been shown to shape the emergent place field properties in CA1 pyramidal cells (Sheffield & Dombeck 2015). One could directly test the effect that dampening these calcium transients, as we have shown here, has on place field properties.

References

Andersen, P., 1960. Interhippocampal impulses. II. Apical dendritic activation of CAI neurons. *Acta physiologica Scandinavica*, 48, pp.178–208.

Arenkiel, B.R. et al., 2008. Genetic control of neuronal activity in mice conditionally expressing TRPV1. *Nat Methods*, 5(4), pp.299–302.

Ariav, G., Polsky, A. & Schiller, J., 2003. Submillisecond precision of the input-output transformation function mediated by fast sodium dendritic spikes in basal dendrites of CA1 pyramidal neurons. *The Journal of neuroscience : the official journal of the Society for Neuroscience*, 23(21), pp.7750–7758.

Azouz, R., Jensen, M.S. & Yaari, Y., 1996. Ionic basis of spike after-depolarization and burst generation in adult rat hippocampal CA1 pyramidal cells. *The Journal of physiology*, 492(1), pp.211–23.

Bamann, C. et al., 2008. Spectral characteristics of the photocycle of channelrhodopsin-2 and its implication for channel function. *Journal of molecular biology*, 375(3), pp.686–94.

Banghart, M. et al., 2009. Photochromic Blockers of Voltage-Gated Potassium Channels. *Angewandte Chemie International Edition*, 48(48), pp.9097–9101.

Beharry, A.A. & Woolley, G.A., 2011. Azobenzene photoswitches for biomolecules. *Chemical Society reviews*, 40(8), pp.4422–37.

Bernard, C. & Johnston, D., 2003. Distance-dependent modifiable threshold for action potential back-propagation in hippocampal dendrites. *Journal of neurophysiology*, 90(3), pp.1807–1816.

Biess, A., Korkotian, E. & Holcman, D., 2011. Barriers to diffusion in dendrites and estimation of calcium spread following synaptic inputs. *PLoS computational biology*, 7(10), p.e1002182.

Birder, L.A. et al., 2002. Altered urinary bladder function in mice lacking the vanilloid receptor TRPV1. *Nature neuroscience*, 5(9), pp.856–60.

Bittner, K.C., Andrasfalvy, B.K. & Magee, J.C., 2012. Ion channel gradients in the apical tuft region of CA1 pyramidal neurons. *PloS one*, 7(10), p.e46652.

Bloodgood, B.L. & Sabatini, B.L., 2007. Nonlinear regulation of unitary synaptic signals by CaV(2.3) voltage-sensitive calcium channels located in dendritic spines. *Neuron*, 53(2), pp.249–60.

Boyden, E.S. et al., 2005. Millisecond-timescale, genetically targeted optical control of neural activity. *Nature neuroscience*, 8(9), pp.1263–8.

Branco, T., Clark, B.A. & Häusser, M., 2010. Dendritic discrimination of temporal input sequences in cortical neurons. *Science (New York, N.Y.)*, 329(5999), pp.1671–5.

Branco, T. & Häusser, M., 2010. The single dendritic branch as a fundamental functional unit in the nervous system. *Current opinion in neurobiology*, 20(4), pp.494–502.

Brunel, N., Hakim, V. & Richardson, M.J.E., 2014. Single neuron dynamics and computation. *Current Opinion in Neurobiology*, 25, pp.149–155.

Cardin, J.A. et al., 2010. Targeted optogenetic stimulation and recording of neurons in vivo using cell-type-specific expression of Channelrhodopsin-2. *Nature Protocols*, 5(2), pp.247–254.

Cash, S. & Yuste, R., 1998. Input summation by cultured pyramidal neurons is linear and

position-independent. *The Journal of neuroscience : the official journal of the Society for Neuroscience*, 18(1), pp.10–15.

Cash, S. & Yuste, R., 1999. Linear summation of excitatory inputs by CA1 pyramidal neurons. *Neuron*, 22(2), pp.383–394.

Cavanaugh, D.J. et al., 2011. Trpv1 reporter mice reveal highly restricted brain distribution and functional expression in arteriolar smooth muscle cells. *The Journal of neuroscience : the official journal of the Society for Neuroscience*, 31(13), pp.5067–77.

Chen, B.L., Hall, D.H. & Chklovskii, D.B., 2006. Wiring optimization can relate neuronal structure and function. *Proceedings of the National Academy of Sciences of the United States of America*, 103(12), pp.4723–8.

Chow, B.Y. et al., 2010. High-performance genetically targetable optical neural silencing by light-driven proton pumps. *Nature*, 463(7277), pp.98–102.

Daoudal, G., Hanada, Y. & Debanne, D., 2002. Bidirectional plasticity of excitatory postsynaptic potential (EPSP)-spike coupling in CA1 hippocampal pyramidal neurons. *Proceedings of the National Academy of Sciences of the United States of America*, 99(22), pp.14512–14517.

Deisseroth, K., 2015. Optogenetics: 10 years of microbial opsins in neuroscience. *Nature neuroscience*, 18(9), pp.1213–1225.

Desjardins, A.E. et al., 2003. The influences of Ih on temporal summation in hippocampal CA1 pyramidal neurons: a modeling study. *Journal of computational neuroscience*, 15(2), pp.131–42.

Euler, T. et al., 2009. Eyecup scope--optical recordings of light stimulus-evoked fluorescence signals in the retina. *Pflügers Archiv : European journal of physiology*, 457(6), pp.1393–414.

Eyal, G. et al., 2014. Dendrites impact the encoding capabilities of the axon. *The Journal of neuroscience : the official journal of the Society for Neuroscience*, 34(24), pp.8063–71.

Ferrante, M., Migliore, M. & Ascoli, G.A., 2013. Functional impact of dendritic branch-point morphology. *The Journal of neuroscience : the official journal of the Society for Neuroscience*, 33(5), pp.2156–65.

Fisher, R.E., Gray, R. & Johnston, D., 1990. Properties and distribution of single voltage-gated calcium channels in adult hippocampal neurons. *Journal of neurophysiology*, 64(1), pp.91–104.

Fitzpatrick, J.S. et al., 2009. Inositol-1,4,5-trisphosphate receptor-mediated Ca2+ waves in pyramidal neuron dendrites propagate through hot spots and cold spots. *The Journal of physiology*, 587(Pt 7), pp.1439–59.

Fortin, D.L. et al., 2011. Optogenetic photochemical control of designer K+ channels in mammalian neurons. *Journal of neurophysiology*, 106(1), pp.488–496.

Fortin, D.L. et al., 2008. Photochemical control of endogenous ion channels and cellular excitability. *Nature methods*, 5(4), pp.331–338.

Frick, A. et al., 2003. Normalization of Ca2+ signals by small oblique dendrites of CA1 pyramidal neurons. *The Journal of neuroscience : the official journal of the Society for Neuroscience*, 23(8), pp.3243–3250.

Frick, A. & Johnston, D., 2005. Plasticity of dendritic excitability. *Journal of Neurobiology*, 64(1), pp.100–115.

Frick, A., Magee, J. & Johnston, D., 2004. LTP is accompanied by an enhanced local excitability of pyramidal neuron dendrites. *Nature neuroscience*, 7(2), pp.126–135.

Fricker, D. & Miles, R., 2000. EPSP amplification and the precision of spike timing in hippocampal neurons. *Neuron*, 28(2), pp.559–569.

Fujita, Y. & Sakata, H., 1962. Electrophysiological properties of CA1 and CA2 apical dendrites of rabbit hippocampus. *Journal of neurophysiology*, 25, pp.209–22.

Gasparini, S. & Magee, J.C., 2006. State-dependent dendritic computation in hippocampal CA1 pyramidal neurons. *The Journal of neuroscience : the official journal of the Society for Neuroscience*, 26(7), pp.2088–2100.

George, M.S., Abbott, L.F. & Siegelbaum, S.A., 2009. HCN hyperpolarization-activated cation channels inhibit EPSPs by interactions with M-type K(+) channels. *Nature neuroscience*, 12(5), pp.577–84.

Gillessen, T. & Alzheimer, C., 1997. Amplification of EPSPs by low Ni(2+)- and amiloride-sensitive Ca2+ channels in apical dendrites of rat CA1 pyramidal neurons. *Journal of neurophysiology*, 77(3), pp.1639–1643.

Goldberg, J.H. & Yuste, R., 2005. Space matters: local and global dendritic Ca2+ compartmentalization in cortical interneurons. *Trends in neurosciences*, 28(3), pp.158–67.

Golding, N.L., Kath, W.L. & Spruston, N., 2001. Dichotomy of action-potential backpropagation in CA1 pyramidal neuron dendrites. *Journal of neurophysiology*, 86(6), pp.2998–3010.

Häusser, M. & Mel, B., 2003. Dendrites: bug or feature? *Current opinion in neurobiology*, 13(3), pp.372–83.

Helmchen, F., Imoto, K. & Sakmann, B., 1996. Ca2+ buffering and action potential-evoked Ca2+ signaling in dendrites of pyramidal neurons. *Biophysical journal*, 70(2), pp.1069–81.

Hille, B., 2001. *Ion Channels of Excitable Membranes*.

Hoffman, D.A. et al., 1997. K+ channel regulation of signal propagation in dendrites of hippocampal pyramidal neurons. *Nature*, 387(6636), pp.869–875.

Jarsky, T. et al., 2005. Conditional dendritic spike propagation following distal synaptic activation of hippocampal CA1 pyramidal neurons. *Nature neuroscience*, 8(12), pp.1667–76.

Jensen, M.S., Azouz, R. & Yaari, Y., 1994. Variant firing patterns in rat hippocampal pyramidal cells modulated by extracellular potassium. *Journal of neurophysiology*, 71(3), pp.831–9.

Jester, J.M., Campbell, L.W. & Sejnowski, T.J., 1995. Associative EPSP--spike potentiation induced by pairing orthodromic and antidromic stimulation in rat hippocampal slices. *The Journal of physiology*, 484(3), pp.689–705.

Jiang, X. et al., 2015. Principles of connectivity among morphologically defined cell types in adult neocortex. *Science*, 350(6264), pp.9462–9462.

Kamondi, A., Acsády, L. & Buzsáki, G., 1998. Dendritic spikes are enhanced by cooperative network activity in the intact hippocampus. *The Journal of neuroscience : the official journal of the Society for Neuroscience*, 18(10), pp.3919–3928.

Kanemoto, Y. et al., 2011. Spatial distributions of GABA receptors and local inhibition of Ca2+ transients studied with GABA uncaging in the dendrites of CA1 pyramidal neurons. *PloS one*, 6(7), p.e22652.

Klapoetke, N.C. et al., 2014. Independent optical excitation of distinct neural populations. *Nature methods*, 11(3), pp.338–46.

Korkotian, E. & Segal, M., 2006. Spatially confined diffusion of calcium in dendrites of hippocampal neurons revealed by flash photolysis of caged calcium. *Cell Calcium*, 40(5-6), pp.441–449.

Lai, H.C. & Jan, L.Y., 2006. The distribution and targeting of neuronal voltage-gated ion channels. *Nature reviews. Neuroscience*, 7(7), pp.548–62.

Lin, J.Y. et al., 2013. ReaChR: a red-shifted variant of channelrhodopsin enables deep transcranial optogenetic excitation. *Nature neuroscience*, 16(10), pp.1499–508.

Lin, W.-C. et al., 2015. A Comprehensive Optogenetic Pharmacology Toolkit for In Vivo Control of GABAA Receptors and Synaptic Inhibition. *Neuron*, 88(5), pp.879–891.

Lin, W.-C. et al., 2014. Engineering a light-regulated GABAA receptor for optical control of neural inhibition. *ACS chemical biology*, 9(7), pp.1414–9.

Lipowsky, R., Gillessen, T. & Alzheimer, C., 1996. Dendritic Na+ channels amplify EPSPs in hippocampal CA1 pyramidal cells. *Journal of neurophysiology*, 76(4), pp.2181–2191.

Llinás, R. et al., 1968. Dendritic spikes and their inhibition in alligator Purkinje cells. *Science (New York, N.Y.)*, 160(3832), pp.1132–5.

Llinas, R. & Nicholson, C., 1971. Electrophysiological properties of dendrites and somata in alligator Purkinje cells. *Journal of neurophysiology*, 34(4), pp.532–51.

London, M. & Häusser, M., 2005. Dendritic computation. *Annual review of neuroscience*, 28, pp.503–32.

Longair MH, Baker DA, Armstrong JD., 2011. Simple Neurite Tracer: open source software for reconstruction, visualization and analysis of neuronal processes. *Bioinformatics*, 27, pp.2453– 2454.

Losonczy, A. & Magee, J.C., 2006. Integrative properties of radial oblique dendrites in hippocampal CA1 pyramidal neurons. *Neuron*, 50(2), pp.291–307.

Magee, J. & Johnston, D., 1995. Characterization of single voltage-gated Na+ and Ca2+ channels in apical dendrites of rat CA1 pyramidal neurons. *The Journal of Physiology*, 487(1), pp.67–90.

Magee, J.C. & Carruth, M., 1999. Dendritic voltage-gated ion channels regulate the action potential firing mode of hippocampal CA1 pyramidal neurons. *Journal of neurophysiology*, 82(4), pp.1895–1901.

Magee, J.C. & Johnston, D., 1997. A synaptically controlled, associative signal for Hebbian plasticity in hippocampal neurons. *Science (New York, N.Y.)*, 275(5297), pp.209–213.

Magee, J.C. & Johnston, D., 1995. Characterization of single voltage-gated Na+ and Ca2+ channels in apical dendrites of rat CA1 pyramidal neurons. *The Journal of physiology*, 487(1), pp.67–90.

Margulis, M. & Tang, C.M., 1998. Temporal integration can readily switch between sublinear and supralinear summation. *Journal of neurophysiology*, 79(5), pp.2809–2813.

Markram, H. et al., 2015. Reconstruction and Simulation of Neocortical Microcircuitry. *Cell*, 163(2), pp.456–492.

Markram, H. et al., 1997. Regulation of synaptic efficacy by coincidence of postsynaptic APs and EPSPs. *Science (New York, N.Y.)*, 275(5297), pp.213–5.

Metz, A.E. et al., 2005. R-type calcium channels contribute to afterdepolarization and bursting in hippocampal CA1 pyramidal neurons. *The Journal of neuroscience : the official journal of the Society for Neuroscience*, 25(24), pp.5763–73.

Meyer, E., Müller, C.O. & Fromherz, P., 1997. Cable properties of dendrites in hippocampal neurons of the rat mapped by a voltage-sensitive dye. *The European journal of*

neuroscience, 9(4), pp.778–85.

Migliore, M., Ferrante, M. & Ascoli, G.A., 2005. Signal propagation in oblique dendrites of CA1 pyramidal cells. *Journal of neurophysiology*, 94(6), pp.4145–55.

Migliore, M. & Shepherd, G.M., 2002. Emerging rules for the distributions of active dendritic conductances. *Nature reviews. Neuroscience*, 3(5), pp.362–370.

Miyakawa, H. et al., 1992. Synaptically activated increases in Ca2+ concentration in hippocampal CA1 pyramidal cells are primarily due to voltage-gated Ca2+ channels. *Neuron*, 9(6), pp.1163–73.

Mourot, A. et al., 2012. Rapid optical control of nociception with an ion-channel photoswitch. *Nature methods*, 9(4), pp.396–402.

Mourot, A. et al., 2011. Tuning photochromic ion channel blockers. *ACS chemical neuroscience*, 2(9), pp.536–43.

Niemz, M.H., 2004. *Laser-Tissue Interactions*.

Palmer, L.M. et al., 2014. NMDA spikes enhance action potential generation during sensory input. *Nature neuroscience*, 17(3), pp.383–90.

Palmer, L.M. & Stuart, G.J., 2009. Membrane potential changes in dendritic spines during action potentials and synaptic input. *The Journal of neuroscience : the official journal of the Society for Neuroscience*, 29(21), pp.6897–903.

Perkins, K.L. & Wong, R.K., 1995. Intracellular QX-314 blocks the hyperpolarization-activated inward current Iq in hippocampal CA1 pyramidal cells. *Journal of neurophysiology*, 73(2), pp.911–5.

Petersen, C.C.H. & Crochet, S., 2013. Synaptic computation and sensory processing in neocortical layer 2/3. *Neuron*, 78(1), pp.28–48.

Pologruto, T.A., Sabatini, B.L. & Svoboda, K., 2003. ScanImage: flexible software for operating laser scanning microscopes. *Biomedical engineering online*, 2, p.13.

Polosukhina, A. et al., 2012. Photochemical Restoration of Visual Responses in Blind Mice. *Neuron*, 75(2), pp.271–282.

Polsky, A., Mel, B.W. & Schiller, J., 2004. Computational subunits in thin dendrites of pyramidal cells. *Nature neuroscience*, 7(6), pp.621–7.

Purpura, D.P. & Shofer, R.J., 1965. Spike-generation in dendrites and synaptic inhibition in immature cerebral cortex. *Nature*, 206(4986), pp.833–4.

Rall, W., 1959. Branching dendritic trees and motoneuron membrane resistivity. *Experimental Neurology*, 1(5), pp.491–527.

Ramakers, G.M.J. & Storm, J.F., 2002. A postsynaptic transient K(+) current modulated by arachidonic acid regulates synaptic integration and threshold for LTP induction in hippocampal pyramidal cells. *Proceedings of the National Academy of Sciences of the United States of America*, 99(15), pp.10144–9.

Remy, S., Beck, H. & Yaari, Y., 2010. Plasticity of voltage-gated ion channels in pyramidal cell dendrites. *Current Opinion in Neurobiology*, 20(4), pp.503–509.

Remy, S., Csicsvari, J. & Beck, H., 2009. Activity-dependent control of neuronal output by local and global dendritic spike attenuation. *Neuron*, 61(6), pp.906–16.

Sheffield, M.E.J. & Dombeck, D.A., 2015. Calcium transient prevalence across the dendritic arbour predicts place field properties. *Nature*, 517(7533), pp.200–204.

Shitaka, Y. et al., 1996. Basic Fibroblast Growth Factor Increases Functional L-Type Ca2+ Channels in Fetal Rat Hippocampal Neurons: Implications for Neurite Morphogenesis In Vitro. *J. Neurosci.*, 16(20), pp.6476–6489.

Sholl, D.A., 1953. Dendritic organization in the neurons of the visual and motor cortices of the cat. *Journal of anatomy*, 87(4), pp.387–406.

Sjöström, P.J. et al., 2010. Dendritic Excitability and Synaptic Plasticity. *Physiological Reviews*, (November 2009), pp.1–28.

Smith, S.L. et al., 2013. Dendritic spikes enhance stimulus selectivity in cortical neurons in vivo. *Nature*, 503(7474), pp.115–120.

Spencer, W.A. & Kandel, E.R., 1961. ELECTROPHYSIOLOGY OF HIPPOCAMPAL NEURONS: IV. FAST PREPOTENTIALS. *J Neurophysiol*, 24(3), pp.272–285.

Spruston, N. et al., 1995. Activity-dependent action potential invasion and calcium influx into hippocampal CA1 dendrites. *Science (New York, N.Y.)*, 268(5208), pp.297–300.

Staff, N.P. et al., 2000. Resting and active properties of pyramidal neurons in subiculum and CA1 of rat hippocampus. *Journal of neurophysiology*, 84(5), pp.2398–2408.

Stuart, G. & Häusser, M., 2007. *Dendrites*, Oxford University Press.

Stuart, G.J., Dodt, H.U. & Sakmann, B., 1993. Patch-clamp recordings from the soma and dendrites of neurons in brain slices using infrared video microscopy. *Pflügers Archiv : European journal of physiology*, 423(5-6), pp.511–8.

Stuart, G.J. & Häusser, M., 2001. Dendritic coincidence detection of EPSPs and action potentials. *Nature neuroscience*, 4(1), pp.63–71.

Stuart, G.J. & Sakmann, B., 1994. Active propagation of somatic action potentials into neocortical pyramidal cell dendrites. *Nature*, 367(6458), pp.69–72.

Svoboda, K. et al., 1997. In vivo dendritic calcium dynamics in neocortical pyramidal neurons. *Nature*, 385(6612), pp.161–5.

Szobota, S. et al., 2007. Remote control of neuronal activity with a light-gated glutamate receptor. *Neuron*, 54(4), pp.535–45.

Takagi, H., 2000. Roles of ion channels in EPSP integration at neuronal dendrites. *Neuroscience research*, 37(3), pp.167–71.

Talbot, M.J. & Sayer, R.J., 1996. Intracellular QX-314 inhibits calcium currents in hippocampal CA1 pyramidal neurons. *Journal of neurophysiology*, 76(3), pp.2120–4.

Tippens, A.L. et al., 2008. Ultrastructural evidence for pre- and postsynaptic localization of Cav1.2 L-type Ca2+ channels in the rat hippocampus. *The Journal of comparative neurology*, 506(4), pp.569–83.

Tochitsky, I. et al., 2012. Optochemical control of genetically engineered neuronal nicotinic acetylcholine receptors. *Nature chemistry*, 4(2), pp.105–11.

Tran-Van-Minh, A. et al., 2015. Contribution of sublinear and supralinear dendritic integration to neuronal computations. *Frontiers in cellular neuroscience*, 9, p.67.

Trigo, F.F., Corrie, J.E.T. & Ogden, D., 2009. Laser photolysis of caged compounds at 405 nm: Photochemical advantages, localisation, phototoxicity and methods for calibration. *Journal of Neuroscience Methods*, 180(1), pp.9–21.

Trimmer, J.S. & Rhodes, K.J., 2004. Localization of voltage-gated ion channels in mammalian brain. *Annual review of physiology*, 66(1), pp.477–519.

Vetter, P., Roth, A. & Häusser, M., 2001. Propagation of action potentials in dendrites depends on dendritic morphology. *Journal of neurophysiology*, 85(2), pp.926–937.

Volgraf, M. et al., 2006. Allosteric control of an ionotropic glutamate receptor with an optical switch. *Nature chemical biology*, 2(1), pp.47–52.

Waters, J., Schaefer, A. & Sakmann, B., 2005. Backpropagating action potentials in neurones: Measurement, mechanisms and potential functions. *Progress in Biophysics and*

Molecular Biology, 87(1 SPEC. ISS.), pp.145–170.

Wathey, J.C. et al., 1992. Computer simulations of EPSP-spike (E-S) potentiation in hippocampal CA1 pyramidal cells. *The Journal of neuroscience : the official journal of the Society for Neuroscience*, 12(2), pp.607–618.

Wei, D.-S., 2001. Compartmentalized and Binary Behavior of Terminal Dendrites in Hippocampal Pyramidal Neurons. *Science*, 293(5538), pp.2272–2275.

Williams, S.R., 2004. Spatial compartmentalization and functional impact of conductance in pyramidal neurons. *Nature neuroscience*, 7(9), pp.961–7.

Wong, R.K., Prince, D.A. & Basbaum, a I., 1979. Intradendritic recordings from hippocampal neurons. *Proceedings of the National Academy of Sciences of the United States of America*, 76(2), pp.986–990.

Xu, N. et al., 2012. Nonlinear dendritic integration of sensory and motor input during an active sensing task. *Nature*, 492(7428), pp.247–51.

Yang, S., Emiliani, V. & Tang, C., 2014. The kinetics of multibranch integration on the dendritic arbor of CA1 pyramidal neurons. *Frontiers in cellular neuroscience*, 8(May), p.127.

Yaroslavsky, A.N. et al., 2002. Optical properties of selected native and coagulated human brain tissues in vitro in the visible and near infrared spectral range. *Physics in medicine and biology*, 47(12), pp.2059–73.

Yasuda, R. et al., 2004. Imaging calcium concentration dynamics in small neuronal compartments. *Science's STKE : signal transduction knowledge environment*, 2004(219), p.pl5.

Yizhar, O. et al., 2011. Optogenetics in neural systems. *Neuron*, 71(1), pp.9–34.

Zhang, F. et al., 2007. Multimodal fast optical interrogation of neural circuitry. *Nature*, 446(7136), pp.633–9.